

1 **Possible evidence for variation in magnitude for marsquakes from fallen boulder**  
2 **populations, Grjota Valles, Mars**

3  
4 Jason. R. Brown, Gerald. P. Roberts,

5  
6 Department of Earth and Planetary Sciences, Birkbeck, University of London, WC1E 7HX,  
7 United Kingdom

8  
9 **Abstract**

10

11 Following observations of mobilized boulder trail populations from Cerberus Fossae, Mars,  
12 that have been interpreted as possible evidence of large magnitude marsquakes rupturing  
13 for distances of ~207 km along exposed active faults, additional boulder trail populations  
14 were measured along shorter faults within the region of Grjota Valles (50-150 km length) to  
15 test the hypotheses that (1) these faults are also candidate locations for marsquakes, and  
16 (2) that marsquake magnitude might be smaller, limited by fault dimensions available for  
17 rupture. For a region containing two en echelon graben, boulder trail data define two  
18 anomalies with maxima in (a) boulder trails per kilometer, and (b) maximum width of  
19 boulder trails, one that is ~116 km in length along strike and the other ~70 km in length  
20 along strike. Values for the maxima are 45 trails per km and 5 m mean trail width for the 70  
21 km long anomaly, and 115 trails per km with 5.3 m mean trail width for the 116 km long  
22 anomaly, above background values measured elsewhere along these faults of zero trails  
23 per kilometer with zero boulder trail widths. If combined with published data from Cerberus  
24 Fossae with a ~207 km long anomaly in boulder trails per km (125 trails per km maxima)  
25 and maximum mean boulder trail width (8.5 m maximum trail width), the 3 datasets  
26 suggest correlations between the (a) along-strike length of boulder trail anomalies, (b)  
27 boulder trails per km and (c) maximum boulder trail width. If interpreted as due to single  
28 marsquakes, and if the dimensions of these anomalies are a proxy for rupture length,  
29 when combined, one interpretation of this is that boulders have been mobilized by  
30 marsquakes and that the marsquake magnitude is proportional to the along strike length of  
31 the anomalies. In other words, the data suggest that marsquake magnitude, if that is the  
32 cause of the anomalies, is limited by fault length as expected for terrestrial seismically  
33 active faults. Such findings suggest that the Martian surface may have been shaken, in the  
34 very recent past, by large magnitude marsquakes. We discuss this in terms of the  
35 seismicity of Mars.

36

37

## 38 **1 Introduction**

39

40 Given that the diameter of Mars (6,790 km) is much smaller than that of the Earth (12,750  
41 km) it has long been considered that Mars is less geologically active than the Earth  
42 because the internal heat source for volcanism and associated faulting would have been  
43 lost more quickly (see Roberts et al. 2012 for a discussion). However, studies by Antoine  
44 et al. (2010) suggest that endogenic heat sources might well be present within Mars  
45 associated with the Cerberus Fossae fault system. Roberts et al. (2012), using  
46 understanding of natural seismometers on Earth, suggested that large magnitude  
47 marsquakes may have occurred in the recent past along Cerberus Fossae, evidenced by  
48 observations close to faults of anomalies in the density of trails left by mobilized boulders  
49 and boulder trail widths (Figs. 1 and 2). Roberts et al. (2012) showed, for Cerberus  
50 Fossae, that boulder trail densities per kilometre and boulder trail widths increased  
51 systematically from background values along the strike of part of the fault system,  
52 interpreting this as possible evidence that a marsquake had produced ground shaking  
53 responsible for mobilization of the boulders. This study was facilitated by the advent of  
54 HiRISE imagery (High Resolution Imaging Science Experiment onboard the Mars  
55 Reconnaissance Orbiter) whose high resolution (~25 cm pixel sizes) allowed, for the first  
56 time, observations of boulders and boulder trails from orbit, in particular the largest  
57 boulders and trails, and hence the ability to map the characteristics of boulder populations  
58 along the strike of fault systems. Roberts et al. (2012) suggested that boulder populations  
59 mobilized by seismic shaking, in particular the widest boulder trails, would show decreases  
60 in mobilized boulder frequency and boulder size over tens of kilometres or more away  
61 from putative epicentres if produced by single large events, as observed on the Earth (Fig.  
62 1), and evidenced on Mars by the widths of trails in dust left by mobilized boulders. In  
63 contrast, boulder populations mobilised by processes facilitating release of boulders from  
64 steep cliffs, such as melting of ground ice on steep slopes, would produce spatially  
65 uniform boulder trail populations, lacking anomalies with dimensions of tens of kilometres  
66 or more. Measurements presented by Roberts et al. (2012) were consistent only with the  
67 hypothesis of mobilisation by seismic shaking (Fig. 1). Furthermore, the trails in the  
68 underlying sediment left by boulders as they rolled and bounced down slopes suggests  
69 relatively-recent boulder mobilization and hence possible ongoing marsquake activity. This  
70 is because tracks produced by the rovers Spirit and Opportunity were erased over



71 timescales of only days to months (Geissler et al. 2010), due to the passage of dust  
72 storms during the perihelion season, although evidence exists of track preservation for  
73 longer periods of time in locations sheltered from the wind; thus tracks left by boulders  
74 would also be erased, suggesting that preserved examples must be relatively young if the  
75 material is fine enough to be mobilised by the wind. Tracks produced by boulders at  
76 Cerberus Fossae are wider and deeper (several meters, several decimeters) than trails left  
77 by rovers (centimetres, centimetres to millimetres) so presumably it would take longer to  
78 erase them with aeolian processes, but the same arguments apply and it is difficult to  
79 envisage an age as old as, for example,  $10^6 - 10^7$  years for the boulder trails. Roberts et  
80 al. (2012) also pointed out that the geographic dimension of the boulder trail  
81 width/frequency anomaly, along the strike of the fault system, might be indicative of the  
82 magnitude of the marsquake, as is the case on Earth (Keefer 1984). The ~207 km wide  
83 zone of mobilized boulders measured along Cerberus Fossae might be consistent with a  
84 marsquake of moment magnitude ~M7.9 (see Wells and Coppersmith 1994). A marsquake  
85 of this magnitude is not inconsistent with the along strike extent of the faults of Cerberus  
86 Fossae because Vetterlein and Roberts (2009) showed that these faults exhibit continuous  
87 along-strike displacement profiles constraining a fault length of ~325 km, longer than the  
88 implied rupture extent, although Knapmeyer et al. (2006) suggested a maximum  
89 magnitude of 7.6. Vetterlein and Roberts (2010) showed that the  $d_{max}/length$  (measured  
90 as vertical offset, throw, in this example) of the Cerberus Fossae faults was ~0.1-0.001,  
91 similar to those measured on Earth, suggesting that the relationships between slip  
92 dimensions and marsquake magnitude might also be similar to the Earth. The question  
93 that arises is whether other examples exist on Mars where shorter fault lengths are  
94 associated with smaller along-strike extents of boulder trail anomalies, implying smaller  
95 moment magnitudes.

96

97 In this paper we seek to extend our knowledge of possible marsquakes by investigating  
98 whether: (a) other possible examples of boulder trail anomalies can be identified, with  
99 evidence ruling out causes other than marsquakes for their formation, and (b) whether  
100 marsquakes of different magnitudes and hence different epicentral shaking intensities to  
101 mobilise boulders can be inferred. To this end we have studied another set of faults that  
102 are parallel to the southern Cerberus Fossae faults located in the region of Grjota Valles  
103 (Fig. 2). Faults in the vicinity of Grjota Valles offset: (i) planar surfaces that are probably  
104 lava flows, (ii) inliers of older terrain such as hills that protrude upwards through the lava  
105 flows, and (iii) outflow channels that may be of aqueous or volcanic origin associated with

106 volcanism (e.g. Burr et al. 2003, Plescia 2003, Jaeger et al. 2010, Morgan et al. 2013,  
107 Hamilton 2013 for associated examples). This means that the Grjota Valles faults are very  
108 similar morphologically to those along Cerberus Fossae studied by Roberts et al. (2012).  
109 Like the examples from Cerberus Fossae described by Roberts et al. (2012), initial  
110 inspection of down faulted regions in Grjota Valles examples revealed many thousands of  
111 boulder trails made by mobilised boulders that have fallen from fault-controlled cliffs  
112 (Figure 3). However, it is clear from inspection of imagery that the faults associated with  
113 Grjota Valles are segmented (Fig. 2), with segments that are shorter (maximum of 60-80  
114 km) than those associated with Cerberus Fossae (Vetterlein and Roberts 2009, 2010;  
115 Taylor et al. 2013). This combination of features allows us to test: (a) whether anomalies in  
116 boulder trail densities and dimensions occur along the faults and are best explained by  
117 marsquakes, and (b) if they are best explained by marsquakes, whether their dimensions  
118 correlate with the dimensions of fault segments. To this end, we examined all the HiRISE  
119 images (Figures 2 and 3) that were available at the time of the study, to constrain the  
120 extent of boulder trail anomalies; see Fig. 2 b, c & Fig. 2 a). We explain in detail why we  
121 have separated the faults into Boulder Trail Anomaly 1 and Boulder Trail Anomaly 2,  
122 based on boulder trail data, below. We have identified two local maxima in boulder trail  
123 densities (that also correlate with boulder trail width) – one associated with each fault line.  
124 We discuss these in terms of their most likely mode of formation, concluding that  
125 marsquakes may be the most likely cause. We then discuss the results in terms of the  
126 possible occurrence of marsquakes with magnitudes controlled by fault dimensions, while  
127 also considering that the marsquake activity may well be relatively recent.

128  
129 First, we present maps of the fault system containing two en echelon graben/faults, one  
130 which is ~115 km length along strike and the other ~82 km length along strike (Figs. 2, 3  
131 and 4). Secondly, we present data concerning the density of boulder trails per kilometer  
132 and boulder trail widths. After discussing the cause of the boulder trail anomalies,  
133 concluding that marsquakes may be the most likely cause of the boulder trail results, and  
134 explaining why other causes are unlikely, we conclude that with the two new boulder trail  
135 data sets presented in this paper, and the example from Roberts et al. (2012), we have 3  
136 examples where boulder trail anomaly dimensions correlate with fault lengths and by  
137 analogy maximum along-strike rupture extent. Thus, the boulder trail data appear to be  
138 consistent with the interpretation that the boulders were mobilized by seismic shaking  
139 produced by marsquakes, and that boulder-trail data may help reveal the magnitudes of  
140 the marsquakes.

141

## 142 **2 Geological Background**

143

144 The fault system we study is located in the vicinity of Grjota Valles and comprises a ~197  
145 km long set of en echelon graben segments located between latitude N16°10'33, longitude  
146 E160°33'48, and latitude N15°12'10 / longitude E163°40'00. The WNW-ESE orientation of  
147 the graben means that the fractures are sub-radial to the Elysium Mons volcano (Fig. 2 a),  
148 and may be the surface expression of sub-surface dikes. Detailed geological and  
149 geomorphological mapping reveals that the geometry of the faults is consistent with that of  
150 graben, with fault controlled cliffs adjacent to flat-bottomed depressions (Figs. 3, 4 and 5).  
151 MOLA data (Mars Orbiter Laser Altimeter on the Mars Global Surveyor (MGS) spacecraft)  
152 reveal that the vertical offset across the graben, which are exposed on a surface that  
153 slopes from -2100 m elevation to -2400 m elevation from west to east, increases from zero  
154 at the tips of the graben to ~900 m at latitude E162° (Fig. 5). This reveals an  
155 offset/subsidence profile that is typical of faults, with vertical offsets as high as ~900 m,  
156 and a  $d_{max}/length$  ratio (with  $d_{max}$  measured as vertical offset for this example) for the  
157 whole structure of 0.005, within the range measured for terrestrial faults and those on Mars  
158 (Schlische et al. 1996; Vetterlein and Roberts 2010). In detail, the MOLA data constrain  
159 the vertical offset across the graben at 180 locations, and reveal displacement gradients  
160 and  $d_{max}/length$  ratios associated with individual distal and medial fault segments of  
161 0.008-0.026, again similar to values measured on Earth (Vetterlein and Roberts 2010; Fig.  
162 5). The similarity in  $d_{max}/length$  values between faults in Grjota Valles and the Earth  
163 suggest that the material strength is similar in the two regions (Gomez-Rivas et al. 2015).  
164 If the material strength is similar then the relationships between rupture length,  $d_{max}$ ,  
165 stress drop and moment magnitude are also likely to be similar (Ali and Shieh 2013). Thus,  
166 our  $d_{max}/length$  observations support the suggestion that these are faults formed by  
167 similar deformation processes to those on the Earth and it may be possible to infer some  
168 aspects of the seismicity, such as moment magnitude, from observations of surface  
169 deformation.

170

171 The faults can be shown to be relatively recent in that they crosscut pre-existing features  
172 of known, relatively-young age (Fig. 2 and 4). The fossae offset Late Amazonian Cerberus  
173 lavas and older inliers (Tanaka et al. 2005). It is believed that the ages of the youngest  
174 lavas offset on the nearby Cerberus Fossae, assessed by crater counting methods, are  
175 <10 Ma (Head et al. 2003; Hartmann and Berman,; 2000; Vaucher et al. 2006), implying

176 that the fossae, if they are all approximately the same age, are even younger. The ~900 m  
177 offset revealed by MOLA data (Fig. 5), if developed since 10 Ma as implied by crater-count  
178 ages, implies a rate of vertical offset of ~0.09 mm/yr, a value that is similar to well-  
179 documented rift systems on the Earth (Vetterlein and Roberts 2010). The faults also offset  
180 a variety of geomorphic features such as lava plains, older inliers and outflow channels  
181 with stream-lined islands (Figure 2; Burr et al. 2003, Plescia 2003, Jaeger et al. 2010). The  
182 similar features were reported for the faults along Cerberus Fossae (Roberts et al. 2012),  
183 so we suggest a similar mode and age of formation for the faults in Grjota Valles.

184

### 185 **3 Method**

186

187 We mapped parts of the Grjota Valles fault system in detail to ascertain the nature of the  
188 geology of the region and gain an overview of the geomorphic features that the boulders  
189 were associated with (Fig. 4).

190

191 NASA HiRISE images have been accessed using the Planetary Data System (PDS) node  
192 at the University of Arizona (<http://hirise.lpl.arizona.edu/>) (Table 1). They were downloaded  
193 at their highest resolution. The images were imported into Google Earth as geo-referenced  
194 image overlays. At the time of writing, there were eighteen areas covered by HiRISE  
195 imagery within the study area of the Grjota Valles (Fig. 2). However, six of the locations  
196 are covered by two HiRISE images, and one of the images (ESP\_027345\_1955) covers  
197 an area which has 6 fractures, 2 of which were required for this study – meaning 12  
198 images were used in total, with one (ESP\_027345\_1955) split into two images: 6a and 6b.  
199 We believe that the number of images available provide sufficient along-strike coverage of  
200 the structures for our purposes. The ruler tool in Google Earth was used to measure  
201 distances and hence boulder trail lengths and widths, allowing for boulder trail density to  
202 be calculated. Roberts et al. (2012) showed that such measurements reproduce the  
203 dimensions of ground-truthed terrestrial boulders to an extent that is adequate for our  
204 purposes. We also checked distance measurements in ArcGIS, and found that this  
205 provides values that are similar to the values from Google Earth to an extent that does not  
206 affect our conclusions (<1% difference between ArcGIS and Google Earth at the latitudes  
207 we are interested in).

208

209

210 We defined the width of boulder trails as the width between what we term “raised levees”  
211 or “sharp edges” that formed as the boulder traversed across the underlying substrate  
212 (Figure 3 a, b, c and d). We included boulder trails without terminal boulders. We measure  
213 the width of the trail where the trail is widest to exclude measurements where the boulder  
214 was bouncing and leaving a narrower trail. There is cross-image variation in boulder trail  
215 density on HiRISE images. Where one can see the substrate is coarse grained, with  
216 visible boulders, no trails exist. Examples of cross-trail variation are shown in Figure 3 b  
217 and c. Thus, we measured the distance across areas where we could gain continuous  
218 records on regions where the substrate appeared fine-grained, converting the values into  
219 number per kilometer.

220

221 For each HiRISE image we measured the following:

222

223 1) We recorded the location of every boulder trail that we were able to identify in each of  
224 the 13 areas along c. 1.5 km – 6.5 km long transects along the slopes immediately  
225 adjacent to the floors of the graben. (e.g. Fig. 6). These transects were chosen because (i)  
226 they existed at the bases of steep slopes along fault-controlled cliffs, and (ii) fine-grained  
227 deposits (probably aeolian sand and dust) were present that preserved boulder trails. We  
228 did not make measurements where the surface was formed of coarse-grained sediments  
229 (> ~20-50 cm particle size) or on solid rock because such locations would be unlikely to  
230 preserve the passage of mobilized boulders if such motion had occurred. The zig-zag lines  
231 in Figure 6 show (a) that we proceeded in a general along strike direction, not returning to  
232 along strike locations where we had already noted boulder trails, because we were  
233 concerned that this could result in erroneous double-counting of boulder trails in our  
234 inventory, and (b) the exact locations where we measured boulder trail width (blue dots), in  
235 general the widest part of the trail, so we could revisit the locations of measurements at a  
236 later date if needed. Along strike distance was recorded as the longitude of each blue dot  
237 on Figure 6, for conversion into the values of boulder trails per kilometer in Figure 8 using  
238 trigonometry and a conversion factor for degrees longitude into kilometers. In summary,  
239 the along-track lengths of the zig-zag tracks were not used in any calculation, but serve to  
240 record exactly how we traversed the boulder trail population and exactly where we made  
241 measurements. We are confident that we have measured every boulder trail where  
242 densities were relatively low (< ~45 boulder trails per km) because they were clear on the  
243 imagery. However, in places it was difficult to recognize every individual boulder trail at  
244 higher densities because some boulder trails coalesce; in these locations (> ~45 boulder

245 trails per km) we think we may have underestimated the number of boulder trails per km,  
246 but this does not affect our overall conclusions (e.g. Fig. 6, with results in Figs. 7 and 8).  
247 We also note that if the boulder trails were  $< \sim 95$  cm in width they would not have been  
248 resolved on current imagery, so again this may have lead us to underestimate the boulder  
249 trail density, but again this does not affect our conclusions as our hypothesis depends on  
250 the largest mobilised and hence the widest boulders trails (Fig. 1).

251

252 2) We measured the width of the 10 widest boulder trails we could identify in each image,  
253 reporting the mean value, to provide an estimate of the dimensions of mobilized boulders.

254

255 We were aware that measuring distances using a ruler tool in software on pixellated  
256 images can be subjective so the two authors made independent measurements of the  
257 same images, with Figure 7a and 7b showing comparisons between results from the two  
258 authors. These results show that the results are repeatable with results from the two  
259 surveys being broadly comparable within error. The differences between results from the  
260 two authors ( $< 1$  m for the mean value for the 10 widest boulder trails;  $< 10$ - $20$  boulder trail  
261 counts per km) are far smaller than the signals that were measured (between 1 and 5.5 m  
262 for the mean value for the 10 widest boulder trails; between 0 and 100 for the boulder trail  
263 counts per km). Overall, we are confident that our method for measuring the number of  
264 boulder trails and their widths using the ruler tool in Google Earth is robust and repeatable  
265 if others were to make measurements from the same images.

266

## 267 **4 Results**

268

269 The data in Figure 8 shows that there are coincident maxima in boulder trail density and  
270 boulder trail widths along the strike of the faults in Grjota Valles.

271

272 In terms of the spatial variations in boulder trail density along the strike of the fault system,  
273 maxima in boulder trail counts exist at around  $E161.5^\circ$  and  $E162.5^\circ$  longitude. Boulder trail  
274 count values decrease both east and west from these locations along the strike of the  
275 faults towards their lateral terminations. We use these variations to define Boulder Trail  
276 Anomaly 1 and Boulder Trail Anomaly 2 mentioned above and shown in Figure 2c. For  
277 Boulder Trail Anomaly 2 we measured a peak of 45 boulder trail counts per km at  
278  $E161.43^\circ$  longitude, with lower values recorded closer to the east and west tips of the

279 graben. For Boulder Trail Anomaly 1, a peak of 102 counts per km at E162.03° was  
280 measured, again with lower values recorded closer to the east and west tips of the graben.

281

282 We note that values for boulder trails per km exhibit an asymmetric pattern along strike  
283 (Fig. 8 a and b). The westernmost point of Boulder Trail Anomaly 2 exhibits the smallest  
284 number of trails per km at 5 trails per km at E160.57° longitude, with the number of trails  
285 increasing as we follow the fault east, culminating in a peak of 45 counts per km at  
286 E161.43° longitude. This is followed by a sharp decrease in the number of recorded trails,  
287 with 4 per km at E161.74° longitude, giving the graph in Figure 8 an asymmetric  
288 appearance. For Boulder Trail Anomaly 1, measurements begin at E161.76° longitude,  
289 extremely close to the tip of Boulder Trail Anomaly 2, but at a latitude of N15.81°, some 6  
290 km to the south of the last measured point along Boulder Trail Anomaly 2. The first count  
291 along Boulder Trail Anomaly 1 records 30 counts per km at E161.7° followed by a sharp  
292 increase in counts, rising to a peak of 102 counts per km at E162.03° longitude, the  
293 highest count along the entire fault. Further east the number of counts decreases,  
294 dropping to 2 counts per km at E163.63° close to the lateral termination of Boulder Trail  
295 Anomaly 1. Again, these measurements give an asymmetric shape (Fig. 8 b).

296

297 Coincident with boulder trail counts per km, there are maxima in boulder trails widths, with  
298 mean values again increasing from close to zero near tips of the structures towards  
299 maximum values (Figs. 8a and 8c). This shows that the areas of high boulder trail density  
300 also have the widest boulder trails (compare Figs. 8b and 8c). Again we note an  
301 asymmetry along strike of the graben for the boulder trail width data. The widest mean  
302 boulder trail width along Boulder Trail Anomaly 2 was ~5 m, and this measurement was  
303 recorded in the region exhibiting the highest number of boulder trails at E161.43°  
304 longitude. As with boulder trails per km, a sharp decrease in the mean width of boulder  
305 trails is observed as we progress west along the fault, with a mean trail width of 1.4 m  
306 being recorded in the region where only four boulder trails were located (E161.76°).  
307 Boulder Trail Anomaly 1 also clearly exhibits the aforementioned relationship, with a  
308 maximum mean boulder trail width of ~ 5 m located in the area of most boulder trails per  
309 km (102), and from this peak the mean width of trails drops to 1.7 m at E163.62°, an area  
310 where only 2 boulder trails per km were recorded (Fig. 8d). Note that for Boulder Trail  
311 Anomaly 1, both the boulder trail width and boulder counts per kilometer, if extrapolated  
312 along strike, have maximum values near to longitude E162.5°, a location where the  
313 surface expression of the fault appears to be non-existent due to the presence of tips to

314 individual graben (see Fig. 2 b, c); a flat plain separates two graben at this location, and  
315 we discuss the possible reasons for this later in the paper. We also note that there does  
316 not appear to be an obvious correlation between the vertical offset across the graben and  
317 the number of boulder trails per km or the mean value for the size of the 10 widest boulder  
318 trails (see locations A and B in Figure 8); again this is discussed later in the paper.

319

## 320 **5 Discussion**

321

322 Results from Grjota Valles show geographically coincident maxima in boulder trail density  
323 per km and boulder trail widths along the graben. This type of observation was used by  
324 Roberts et al. (2012) to suggest that the most plausible mechanism to mobilize such  
325 populations of boulders is seismic shaking associated with palaeomarsquakes (see Figure  
326 1). They concluded this because boulders mobilized by seismic shaking would “display the  
327 classic pattern associated with earthquakes where both the frequency of boulder falls and  
328 boulder sizes decrease away from the epicenter and the location of coseismic surface  
329 faulting, due to localized ground shaking (Keefer 1984)” (Fig. 1). However, there are other  
330 possible mechanisms that may have mobilised the boulders, and we discuss each of them  
331 in turn below.

332

333 1) *Release of boulders by melting ice.* A plausible hypothesis is that boulders are held on  
334 the steep slopes and cliffs associated with the graben by water or CO<sub>2</sub> ice. Any diurnal,  
335 seasonal or longer-term warming might melt the ice and release the boulders. Roberts et  
336 al. (2012) suggest that boulders mobilized in this way would show “a random spatial  
337 pattern of maximum boulder sizes” when sampled over “tens to hundreds of kilometers”  
338 (Figure 1). However, our measurements show clear local maxima in boulder trail widths  
339 and boulder trail density per kilometer that are geographically coincident (Figure 8). Note,  
340 the actual mean value for the widest boulder trail may be larger if measured from a larger  
341 population of trails, so there is an element of circular reasoning here. However, even with  
342 this caveat, these results, with geographically-coincident maxima in values for the two  
343 variables (Figure 8), are not what would be expected of the mechanism of boulder release  
344 by melting ice. Furthermore, it is unclear how this process could control the dimensions of  
345 boulders recorded by the boulder trail widths, and, like Roberts et al. (2012), (their Figure  
346 10), we have found no evidence for differing joint-spacing in the bedrock to explain the  
347 variable maximum boulder sizes implied by the variable maximum boulder trail widths,  
348 although the restriction of image resolution means we cannot rule it out. Furthermore,



349 persistent CO<sub>2</sub> frost may not be plausible at this latitude (Piqueux et al., 2016), so it may  
350 be unrealistic to expect such frost to hold boulders on slopes. For these reasons so we  
351 reject this hypothesis.

352

353 *2) The effect of local differences lithology and hence weathering/erosion.* A plausible  
354 hypothesis is that different lithologies might be more or less prone to erosion and this  
355 might control the number and sizes of boulders released from the steep slopes and cliffs  
356 associated with the graben. Our geological mapping shows no obvious changes in  
357 lithology of the rocks forming the walls to graben (Figure 4). We have also examined  
358 available THEMIS (Thermal Emission Imaging System) and CRISM (Compact  
359 Reconnaissance Imaging Spectrometer for Mars) data to try to ascertain if local lithological  
360 changes correlate with the measured maxima in boulder trail widths that are coincident  
361 with the measured maxima in boulder trails per kilometer. The CRISM data, although  
362 having limited lateral extent and hence availability, appear to show no obvious change in  
363 lithology of the rocks forming the walls to graben with regard to oxidised iron minerals,  
364 mafic mineralogy, hydroxylated silicates, bound water or water ice and CO<sub>2</sub> ice  
365 (Supplementary Figure S1). The THEMIS data, including both night time and daytime  
366 infrared measurements, provide complete spatial coverage of the area studied, and,  
367 although probably saturated in the images we show, again show no obvious change in  
368 lithology of the rocks forming the walls to the graben, highlighting only that the walls of the  
369 graben appear to formed of bedrock (Supplementary Figures S2 and S3), as confirmed by  
370 the clear stratigraphic layers in the HiRISE images (Figure 4). The HiRISE data show a  
371 layered stratigraphy in the graben walls that are presumably lava flows and possibly  
372 sedimentary layers formed by weathering erosion and aeolian processes between lava  
373 flow events. There appears to be little if any obvious differences in stratigraphy between  
374 different HiRISE images (Figure 4). Thus, as we have not identified any changes in  
375 lithology, despite having a variety of data sources, we reject the hypothesis that different  
376 lithologies might be more or less prone to erosion and this might control the number and  
377 sizes of boulders released from the steep slopes and cliffs associated with the graben. We  
378 also have no evidence to address the possibility that that wind helps dislodge rocks, either  
379 directly or by forcing sand and dust into cracks, wedging them open, in a way that  
380 produces the regional variations in boulder trail frequency and size shown in Figure 8.

381

382 *3) Higher cliffs could supply more boulders.* A plausible hypothesis is that the higher  
383 frequency of boulder trails we have measured in some HiRISE images might be explained

384 by proximity to higher cliffs that have a greater number of loose boulders available for  
385 mobilization. However, it is not just the cliffs that supply boulders. The talus at the bases of  
386 the cliffs also contains boulders that could be mobilised as they are likely to be sitting on  
387 slopes that are close to their angle of repose. Thus, the combined height of the cliffs and  
388 the talus should be taken into account. Also, the talus slopes are all likely to be close to  
389 their angle of repose, and the cliffs appear to be close to vertical, so variations in local  
390 slope is probably not a variable that needs to be considered. Although it is not possible to  
391 measure the heights and slopes of all the individual cliffs or individual talus cones,  
392 because (a) MOLA spot spacing of ~300 m is too coarse (Supplementary Figure S4), (b)  
393 shadow width and solar incidence angle cannot be used to define vertical height  
394 differences via trigonometry, because the horizontal extents of talus slopes vary between  
395 different examples (Supplementary Figure S5), and (c) stereo HiRISE pairs to make local  
396 digital elevation models are not available for the majority of HiRISE locations in the study  
397 area, it is possible to measure the total offset across the faults controlling the graben walls  
398 using the MOLA data (Figures 5 and 8). For example, locations A and B in Figure 8 show  
399 similar values for boulder trails per kilometer and boulder trail widths, but very different  
400 combined heights of the fault-controlled cliffs plus talus slope height defined by the total  
401 offset measured with MOLA data. Thus, if the vertical extent of cliffs plus associated talus  
402 slopes provides more candidate boulders for mobilization, this does not tally with our  
403 measurements of maxima in boulder trail frequency. Also, this hypothesis does not explain  
404 why the widths of boulder trails correlate with the frequency of boulder trails. Thus, for  
405 these two reasons we reject this hypothesis.

406

407 4) *Boulder mobilization caused by nearby impacts.* A plausible hypothesis is that formation  
408 of nearby impact craters could have produced ground shaking that mobilized the boulders.  
409 We have examined all impact craters within ~ 50 km across strike of the graben we have  
410 studied. A ~4 km diameter crater is located at Latitude 15.618° and Longitude 162.183°,  
411 close to the area with maxima in boulder trail frequency and boulder trail width. However,  
412 the ejecta blanket from this crater has been eroded by an outflow channel, so the crater  
413 pre-dates the outflow. The outflow channels pre-date the graben evidenced by cross-  
414 cutting relationships (see Vetterlein and Roberts 2009 for a description of how cross-  
415 cutting relationships are ascertained), and the boulder trails post-date graben formation.  
416 Hence, this crater is too old to have been involved in boulder mobilization. Smaller craters  
417 (~ 40 m diameter) exist within a few hundred metres of the graben in the vicinity of the  
418 maxima in boulder trail frequency and width (Supplementary Figure S6). However, these

419 craters, although having a relatively young appearance at first sight, due to the existence  
420 of dark, presumably relatively dust-free material within them, are in fact partially filled with  
421 aeolian dunes. The dunes were mobilized by the wind, yet the boulder trails have not been  
422 destroyed by the action of wind, suggesting that they are younger than the dunes. Thus, if  
423 the rate of aeolian processes is similar between these craters and the graben floors, these  
424 small craters are also ruled out as candidates for producing the ground shaking that  
425 mobilized the boulders. Thus, as no candidate craters have been identified we rule out this  
426 hypothesis, but note that this is dependent on our assumption that the rate of aeolian  
427 processes is similar between craters and the graben floors.

428

429 5) *Track density may correlate with better preservation and/or lower degradation rather*  
430 *than more abundant formation.* A plausible hypothesis is that the boulder trails may be  
431 degraded by erosion, and that degradation may vary spatially influencing the number of  
432 trails that are preserved, and the widths that are measured. To assess this we have  
433 compared boulder trail widths with the dimensions of the boulders that formed them  
434 (Figure 3 d). We assume that the boulders are more resistant to wind erosion than the  
435 underlying dust surfaces that they have rolled over, and will maintain their original  
436 dimensions. Thus, a comparison between the dimensions of the boulders and the trails  
437 should reveal whether trail widths have been altered by wind erosion. We have found that  
438 in areas of both high and low boulder trail density and width, the widths of the boulder  
439 trails are indistinguishable in width from the width of the boulders that formed them. This  
440 suggests the trails are not eroded to an extent that radically alters their widths or  
441 preservation. That the trails have not been significantly degraded by wind erosion is  
442 consistent with the preservation of raised levees produced by the motion of boulders,  
443 evidenced by variation in percentage grayscale for individual pixels in the images (Figure 3  
444 d (v)). Thus, we reject this hypothesis.

445

446 6) *Variation in incidence angle of the images makes trails difficult to see.* A plausible  
447 hypothesis is that recognition of trails may be hindered by, for example, the solar  
448 incidence angles in the HiRISE images. Supplementary Figure S7 shows that solar  
449 incidence angles are very similar for the images we have studied. Also, our qualitative  
450 assessment after studying many examples is that individual boulder trails are as clear on  
451 images with low boulder trail frequency and width as they are on images with high boulder  
452 trail frequency and width. For these reasons we reject this hypothesis.

453

454 7) *The accumulation of boulder trail populations may have developed from multiple single*  
455 *rock falls through time.* As single rockfalls have been observed on repeat imagery (for  
456 example see [https://www.msss.com/mars\\_images/moc/2005/09/20/bouldertracks/](https://www.msss.com/mars_images/moc/2005/09/20/bouldertracks/) which  
457 appears to show possible bounce marks and longer lived debris flow channels) then a  
458 plausible hypothesis is that repeated single rock-falls could be responsible for the  
459 populations of boulder trails, perhaps triggered by many small marsquakes or many  
460 releases of boulder by melting ice or other processes. Our qualitative observation on this  
461 point is that the morphology of the boulder trails appears to be identical across the many  
462 thousands of boulder trails we have observed. They appear to have raised levees only a  
463 few decimetres across that are presumably made of dust to coarse sand (Figure 3 d). We  
464 think it is dust to coarse sand because it is susceptible to being disturbed by a rolling  
465 boulder to form a raised levee, and hence we also think it would be susceptible to  
466 subsequent wind erosion (Figure 3 d). We do not think these examples on Mars are  
467 associated with gravel-grade material that would be less susceptible to wind erosion. This  
468 is because we have conducted fieldwork in Iceland where boulder trails have formed in  
469 talus cones on fault scarps made of gravel-grade material (grain size of up to 10-15 cm)  
470 (Supplementary Figure S8). The examples in Iceland lack raised levees and we think this  
471 is due to the relatively-coarse grain-size, and hence interpret the grainsize for the  
472 examples from Mars as dust to coarse sand. The raised levees in the examples from Mars  
473 are, as described above, evidenced by variation in percentage grayscale for individual  
474 pixels in the images with the sun illuminating the raised levees that also produce shadows  
475 (Figure 3 d). The key point is that with clear examples of active aeolian processes on the  
476 graben floors in the form dunes (e.g. Figure 4 a), and the interpreted dust to coarse sand  
477 grainsize, the fact that raised levees are preserved in many thousands of examples  
478 suggests they are young and hence of very similar age. For this reason we reject the  
479 hypothesis of incremental formation of the boulder trail populations by addition of single  
480 boulder falls, although we admit that this is supported only by qualitative observations.  
481 Rather, we suggest that two events have formed the two boulder trail populations shown in  
482 Figure 8. Note that if we are incorrect about the levees, and in fact the population of  
483 boulder trails contains examples of individual boulder trails with very different ages, then  
484 the population could have accumulated through many smaller rock falls, invalidating our  
485 large magnitude marsquake interpretations, but we suggest that our evidence appears to  
486 point to the opposite interpretation, consistent with large magnitude marsquakes.

487

488 8) *Measurements used to define boulder trail anomalies.* A plausible hypothesis is that

489 there may be a problem with our measurements. It may be that the mean width of the 10  
490 widest trails is inadequate to allow comparison of boulder trail populations produced by  
491 mobilization of a sub-set of the population of available boulders, if populations of different  
492 number are considered and they have a power-law or exponential size distribution. One  
493 scenario could be that if more are boulders are drawn from such a population, there will be  
494 more individual large boulders and the mean will be larger, even if the size-frequency  
495 distribution is identical. We have been unable to define the number, as we have not  
496 counted the total number of boulders in each location, but it is perhaps likely that the  
497 extremely large numbers of candidate boulders for mobilization at every location means  
498 that the population sizes are not significantly different. Our results stand if we assume that  
499 the number of boulders in the population is identical between locations, but clearly we  
500 have not been able to rule out this possibility.

501

502 After consideration of the alternative scenarios described above, we conclude, following  
503 Roberts et al. (2012), that a plausible explanation for the boulder trail data we present  
504 herein may be that the boulders were mobilized by seismic shaking associated with  
505 palaeomarsquakes, with shaking, and hence boulder mobilization, decreasing with  
506 distance from the epicentres. Thus, although, perhaps not completely proven, as we have  
507 not ruled out some alternative hypotheses, we think it worthwhile to explore the  
508 implications that arise if this marsquake hypothesis is correct.

509

510 We note that the marsquake interpretation requires one of our interpreted marsquake  
511 ruptures to cross an area where there is no surface offset. We note that it is common for  
512 ruptures to jump between active faults that are not physically continuous in terrestrial  
513 earthquakes and provide an example of this in Supplementary Figure S9 (see Livio et al.  
514 2016). The same may apply on Mars. This is important to note, because, like on the Earth,  
515 estimates of maximum marsquake magnitude may be erroneously small if it is assumed  
516 that ruptures can be confined to single active faults.

517

518 If our conclusion that the boulder populations were mobilized by marsquakes is correct,  
519 the observation that the results of this study are similar to those of Roberts et al. (2012),  
520 suggests that we should discuss data from that paper alongside those in this paper to  
521 broaden our understanding of the potential significance of the boulder trail populations  
522 (Fig. 9). An obvious difference between the data sets is that the hump-shaped anomalies  
523 extend over ~207 km for Cerberus Fossae (Roberts et al. (2012), whilst those that emerge

524 from this paper extend over ~116 km for Boulder Trail Anomaly 1, and ~70 km for Boulder  
525 Trail Anomaly 2 (Fig. 9). Roberts et al. (2012) suggested that the along strike extent of  
526 seismic shaking great enough to mobilise boulders on Earth is approximately the same as  
527 the along strike extent of surface faulting for the earthquake ruptures, consistent with  
528 observations from the 2009 Mw 6.3 earthquake near L'Aquila, Italy. Roberts et al. (2012)  
529 also tentatively mapped possible surface rupture extent using HiRISE images for Cerberus  
530 Fossae, and observations were consistent with the hypothesis. Following this, although we  
531 have not been able to map rupture extent in the present example, and the 1:1 ratio  
532 between rupture length and the dimensions of areas with mobilized boulders on Earth is  
533 only approximate, if the along strike extent of the hump-shaped anomalies in boulder trail  
534 data are taken as proxies for along strike rupture extent, the implied moment magnitudes  
535 for the palaeomarsquakes, assuming that the humps result from single events, may be in  
536 the range of ~Mw 7.3-7.8 (Fig. 9d). It should be noted that our assumption that the  
537 anomalies formed in single events and not multiple small events (see the discussion in  
538 Point 7 above), mean that these magnitudes should be considered as maximum values.  
539 However, our assumptions are supported indirectly by the observation that  $d_{max}/length$   
540 ratios for the Martian faults examined herein (0.026-0.008; Figure 5) are similar to those  
541 measured on the Earth (0.1-0.001; see Vetterlein and Roberts 2010 for a review). In turn,  
542 this implies that material strength and the relationships between rupture length,  $d_{max}$ ,  
543 stress drop and moment magnitude are also likely to be similar to those on the Earth  
544 (Gomez-Rivas et al. 2015; Ali and Shieh 2013). Moment magnitudes in the range of ~Mw  
545 7.3-7.8 implies events whose seismic shaking would be widely felt/detected on the Martian  
546 surface by seismometers such as those associated with the Interior Exploration using  
547 Seismic Investigations, Geodesy and Heat Transport (InSIGHT) mission. However, also  
548 note that we may be mistaken in our assumption that along strike extent of the hump-  
549 shaped anomalies in boulder trail data is a proxy for along strike rupture extent, as  
550 unfortunately, unlike Roberts et al. (2012), we have been unable to map surface rupture  
551 for example in Grjota Valles. Gravity on Mars is ~38% compared to that of the Earth so  
552 less force might be needed to mobilise boulders, but it is hard to be precise as this  
553 depends on how each boulder was attached and detached, and whether each boulder was  
554 mobilized by vertical or horizontal accelerations (see Supplementary Figure S5 c-h for an  
555 explanation). However, it is possible that the along strike extent of the hump-shaped  
556 anomalies in boulder trail data may be greater than along strike rupture extent, so this is  
557 another reason why the estimates of ~Mw 7.3-7.8 should be considered maximum values.  
558 Nonetheless, if we use the observation that boulder trail anomalies have similar along

559 strike dimensions to suggested surface ruptures for the Cerberus Fossae example  
560 (Roberts et al. 2012), the results point towards the conclusion that a variety of magnitudes  
561 of palaeomarsquake may have been detected, with larger magnitudes on the Cerberus  
562 Fossae fault system which displays fault segments lengths of several hundred kilometers  
563 from geomorphic observations of offset features, and smaller magnitudes on the Grjota  
564 Valles system where segmented lengths are in the range of 50-100 km, again from  
565 geomorphic observations (Fig. 2 and Fig. 9). This correlation between fault dimensions  
566 and dimensions of areas affected by putative seismic shaking adds further support, albeit  
567 indirect, for our interpretation of palaeomarsquakes.

568

569 Furthermore, we suggest that it may be possible to infer details of how well seismic  
570 shaking is recorded by our natural seismometer, that is, the boulder trail population data.  
571 Fig. 10a compares the three faults; Boulder Trail Anomaly 1, Boulder Trail Anomaly 2 and  
572 Roberts et al.'s (2012) fault, plotting boulder trails per km versus boulder trail width. A  
573 positive relationship exists between boulder trails per km and the width of boulder trails,  
574 with a greater number of boulder trails corresponding to a greater width of boulder trails.  
575 However, it is interesting to note that the data appear to saturate. Data from Roberts et al.  
576 (2012) increase from zero to ~5-8 m for the mean value of the 10 widest boulder trails over  
577 the range of ~0-50 boulder trails per km, and then appear to flatten out at larger values  
578 with the value of ~5-8 m for the mean value of the 10 widest boulder trails maintained over  
579 the range of ~50-125 boulder trails per km. One interpretation of this is that the natural  
580 seismometer is saturating, and unable to record shaking that would mobilise larger  
581 boulders. It may be that boulders > 5 - 8 m are not available in great numbers on the fault-  
582 controlled slopes, perhaps controlled by joint spacing or layer thicknesses in the rocks.  
583 Furthermore, we note that the Fig. 10 b shows a positive relationship between the along  
584 strike length of the boulder trail anomaly and the maximum value for boulder trails per km  
585 recorded. This may be interpreted to suggest that maximum ground acceleration may  
586 increase with marsquake magnitude. However, we note that from the sparse data we  
587 have, constrained with only 3 data points, that the trend again flattens-out, and that we  
588 might expect the example from Roberts et al. (2012) to have more than the ~120 boulder  
589 trails per km recorded. We suggest that again the natural seismometer might be  
590 saturating, perhaps because once a value of ~45 boulder trails per km is exceeded it  
591 becomes difficult in some cases to identify every single boulder trail because they appear  
592 to coalesce on the images. The preceding text pertaining to performance of our natural  
593 seismometer is speculative. However, we note that if correct, it implies that boulder trail

594 populations may not be effective in measuring the effects of marsquakes at the largest  
595 magnitudes because the measurements may be saturated.

596

597 As a final point of discussion we note that profiles of data for boulder trail anomalies 1 and  
598 2 are asymmetric (Figures 8 and 9), with the steepest gradients closest to the en echelon  
599 fault step-over (labelled A in Figure 9a) between these two fault segments. For faults on  
600 the Earth we note that displacement gradients steepen in the step-over zones between  
601 interacting faults (Jackson et al. 2002). The asymmetry in boulder trails populations may,  
602 perhaps, be related to this. A speculative interpretation might be that slip-distributions for  
603 each of the individual marsquake ruptures that produced these boulder-trail anomalies  
604 were skewed towards the tips of fault segments, so that the largest coseismic  
605 displacements, and hence highest levels of ground acceleration, were located close to the  
606 en echelon step-over between the fault segments, as occurs on the Earth (Faure Walker  
607 et al. 2009).

608

609 Overall, the boulder trail data presented in this paper are intriguing, but not conclusive.  
610 Clearly, what is needed is for a seismometer placed on the surface of Mars to actually  
611 record a marsquake before we can conclude that seismicity is present (see Lorenz et al.  
612 2017 who suggest that seismometer data from the Viking missions may have already  
613 detected seismic shaking, and data acquisition planned for the InSIGHT seismometer  
614 mission to Mars of 2018-19). The data herein may suggest relatively large events, perhaps  
615 up to Mw 7.3-7.8. However, magnitudes >Mw 7.6 seems improbable given the analysis of  
616 Knapmeyer et al. (2006). We point out that the uncertainty indicated by the spread in the  
617 data supporting Figure 9d allow our interpretation to be consistent with the estimate in  
618 Knapmeyer et al. (2006). Nonetheless, events as large Mw 7.6 would have recurrence  
619 intervals that are very long (perhaps hundreds to thousands of years), much longer than  
620 the lifetime of a seismometer. The likelihood of measuring such an event with the InSIGHT  
621 seismometers is, of course, very small. However, if like on the Earth, for every large event  
622 there are hundreds to thousands of smaller events with shorter return times following  
623 Gutenberg-Richter b-value scaling (e.g. Knapmeyer et al. 2006), it may be that one of  
624 these smaller events is more likely to be recorded by the InSIGHT seismometers.. The  
625 annual detectability of such events by the InSIGHT instruments was investigated by Taylor  
626 et al. (2013), and they conclude that between  $1.5 \times 10^0$  and  $1.9 \times 10^5$  events would be  
627 detected, depending on the maximum defined event size; our results provide new  
628 information on the possible maximum event sizes. The ideas in this paper can and should



629 be tested by data provided by the InSIGHT mission. The data in this paper suggest that  
630 the Martian surface is not completely still; instead they hint that the Martian surface may  
631 well have be shaken by large magnitude marsquakes in the very recent past.

## 632 **6 Conclusions**

633

634 We have studied two faulted areas in the vicinity of Grjota Valles (Boulder Trail Anomaly 1  
635 and Boulder Trail Anomaly 2), measuring the densities and widths of boulder trails created  
636 by boulders falling from fault-controlled cliffs. These data are consistent with previous  
637 results (Roberts et al. 2012) in that the most parsimonious interpretation is that boulders  
638 have been mobilized by seismic shaking associated with palaeomarsquakes in the recent  
639 past. Our conclusions can be tested with data from the InSIGHT mission that is on the  
640 Martian surface at the time of writing. For now, we report that a region containing two en  
641 echelon graben/faults with similar  $d_{max}/length$  ratios to those from the Earth, boulder trail  
642 data define two maxima in (a) boulder trails per kilometer and (b) maximum width of  
643 boulder trails, one which is ~116 km length and the other ~70 km length. Values for the  
644 maxima are 45 trails per km and 5 m maximum trail width for the 70 km long anomaly, and  
645 115 trails per km with 5.3 m maximum trail widths for the 116 km long anomaly, above  
646 background values of zero trails per kilometer with zero boulder trail widths. Combined  
647 with published data from Cerberus Fossae where the a ~207 km long anomaly in boulder  
648 trails per km (125 trails per km maxima) and maximum boulder trail width (8.5 m maximum  
649 trail width), the 3 datasets suggest correlations between the along-strike length of boulder  
650 trail anomalies, boulder trails per km and maximum boulder trail width. Implied moment  
651 magnitudes, derived by using the along strike dimensions of boulder trail anomalies as  
652 proxies for rupture extent, could be as large as Mw 7.3-7.8, values that we expect to be  
653 accompanied by much more frequent seismic activity at lower moment magnitudes.

654

## 655 **Acknowledgements**

656

657 We acknowledge STFC grant ST/K006037/1 that funded some of this work. We  
658 acknowledge the HiRISE teams (NASA/JPL/University of Arizona) for providing images  
659 and the MOLA team for topographic data. We thank Jonny Roberts for his help with the  
660 fieldwork in Iceland. The data used in this paper are appropriately cited in the references  
661 section of this paper. We thank the reviewers and Associate Editor for their detailed and  
662 constructive comments.

663

664 **References**

665

666 Ali, W., Shieh, S, (2013) Earthquake repeat time, stress drop, type of slip and earthquake  
667 magnitude. *J. Geol. Geosci.*, 2:2. <http://dx.doi.org/10.4172/2329-6755.1000118>

668 Antoine, R., T. Lopez, D. Baratoux, M. Rabinowicz, K. Kurita, (2010) Thermal analysis of  
669 fractures at Cerberus Fossae, Mars: Detection of air convection in the porous debris  
670 apron. *Icarus*, 214 (2): 433-446.

671 Berman, D. C. and Hartmann W. K. (2002) Recent fluvial, volcanic, and tectonic activity on  
672 the Cerberus Plains of Mars. *Icarus* 159, 1-17.

673 Burr, D.M., J. A. Grier, A. S. McEwen, L. P. Keszthelyi, (2002) Repeated aqueous flooding  
674 from the Cerberus Fossae: Evidence for very recently extant, deep groundwater on  
675 Mars. *Icarus* 159: 53-77.

676 Burr, D. M., A. S. McEwen, S. E. H. Sakimoto (2002) Recent aqueous floods from the  
677 Cerberus Fossae, Mars. *Geophysical Research Letters* 29 (1): 13-1-13-4.

678 Faure Walker J., G.P. Roberts, P.A. Cowie, I. Papanikolaou, A.M. Michetti, P. Sammonds  
679 and R. Phillips (2009) Horizontal strain-rates and throw-rates across breached relay-  
680 zones, central Italy: implications for the preservation of throw deficits at points of  
681 normal fault linkage. *Journal of Structural Geology*, 31, 1145-1160,  
682 doi:10.1016/j.jsg.2009.06.01

683 Geissler, P. E., R. Sullivan, M. Golombek, J. R. Johnson, K. Herkenhoff, N. Bridges, A.  
684 Vaughan, J. Maki, T. Parker, J. Bell (2010) Gone with the wind: Eolian erasure of the  
685 Mars Rover tracks. *Journal of Geophysical Research*: 115.

686 Gomez-Rivas, E., Griera, A., Llorens, M.-G. (2015) Fracturing of ductile anisotropic  
687 multilayers: influence of material strength. *Solid Earth*, 6, 497-514, 2015  
688 <https://doi.org/10.5194/se-6-497-2015>.

689 Hamilton, C. W., Flood lavas associated with the Cerberus Fossa 2 unit in Elysium Planitia,  
690 Mars. (2013) Abstract for the 44<sup>th</sup> Lunar and Planetary Science Conference.

691 Hartmann, W. K. and Berman D. C. (2000) Elysium Planitia lava flows: Crater count  
692 chronology and geological implications. *Journal of Geophysical Research* 105 (E6):  
693 15011-15,025.

694 Head, J.W., L. Wilson, K. L. Mitchel (2003), Generation of recent massive water floods at  
695 Cerberus Fossae, Mars by dike emplacement, cryospheric cracking, and confined  
696 aquifer groundwater release. *Geophysical Research Letters* 30 (11).

697 Jackson, C. A. L., R. L. Gawthorpe, I. R. Sharp (2002) Growth and linkage of the East  
698 Tanka fault zone, Suez rift: structural style and syn-rift stratigraphic response.  
699 *Journal of the Geological Society*. 159: 175-187.

700 Jaeger, W. L., Keszthelyi, K. P., Skinner, J. A., Milazzo, M. P., McEwen, A. S., Titus, T. N.,  
701 Rosiek, M. R., Galuszka, D. M., Howington-Kraus, E., Kirk, R. L., and HIRISE Team,  
702 (2010), Emplacement of the youngest flood lava on Mars: a short turbulent story.  
703 *Icarus*, 205, 230-243, doi:10.1016/j.icarus.2009.09.011.

704 Keefer D. K. (1984) Landslides caused by earthquakes. *Geological Society of America*  
705 *Bulletin*. 95: 406-421.

706 Knapmeyer, M., Oberst, J., Hauber, E., Wahlisch, M., Deuchler, C., Wagner, R. (2006)  
707 Working models for spatial distribution and level of Mars' seismicity. *Journal of*  
708 *Geophysical Research*, Vol. 111, E11006, doi:10.1029/2006JE002708,

709 Livio F; Michetti AM; Vittori E; Gregory L; Wedmore L; Piccardi L; Tondi E; Roberts G;  
710 Blumetti AM; Bonadeo L; Brunamonte F; Comerci V; Di Manna P; Ferrario MF; Faure  
711 Walker J; Frigerio C; Fumanti F; Guerrieri L; Iezzi F; Leoni G; McCaffrey K; Mildon Z;  
712 Phillips R; Rhodes E; Walters RJ; Wilkinson M (2016) [Surface faulting during the](#)  
713 [August 24, 2016, central Italy earthquake \(Mw 6.0\): Preliminary results](#), *Annals of*  
714 *Geophysics*, 59, . doi: 10.4401/ag-7197

715 Lorenz, R. D., Nakamura, Y., Murphy, J. R. (2017) [Viking-2 Seismometer Measurements](#)  
716 [on Mars: PDS Data Archive and Meteorological Applications](#). *Earth and Space*  
717 *Science*, 4, 11, p681-688.

718 Morgan, G., Campbell, B. A., Carter, L. M., Plaut, J. J., Phillips, R. J., (2013), 3D  
719 reconstruction of the source and scale of buried young flood channels on Mars.  
720 *Science*, 340, doi: 10.1126/science.1234787.

721 Piqueux, S., A. Kleinböhl, P. O. Hayne, N. G. Heavens, D. M. Kass, D. J. McCleese, J. T.  
722 Schofield, and J. H. Shirley (2016), Discovery of a widespread low-latitude diurnal  
723 CO<sub>2</sub> frost cycle on Mars, *J. Geophys. Res. Planets*, 121, 1174–1189,  
724 doi:10.1002/2016JE005034.

725 Plescia, J. B. (2003) Cerberus Fossae, Elysium, Mars: a source for lava and water.  
726 *Icarus*: 164: 79-95.

727 Roberts, G.P., B. Matthews, C. Bristow, L. Guerrieri, J. Vetterlein (2012) Possible evidence  
728 of paleomarsquakes from fallen boulder populations, Cerberus Fossae, Mars.  
729 *Journal of Geophysical Research*, 117.

730 Schlische, R. W., S. S. Young, R. V. Ackermann, A. Gupta (1996) Geometry and scaling  
731 relations of a population of very small rift-related normal faults: *Geology*, 24: 683-686.

- 732 Tanaka, K. L., J. A. Skinner, T. M. Hare, (2005) Geologic Map of the Northern Plains of  
733 Mars. *Pamphlet to accompany Scientific Investigations Map 2888, USGS for NASA.*  
734 <https://pubs.usgs.gov/sim/2005/2888/>.
- 735 Taylor, J., Teanby, N. A., Wookey, J., (2013), Estimates of seismic activity in the Cerberus  
736 Fossae region of Mars, *Journal of Geophysical Research, Planets*, VOL. 118, 2570-  
737 2581, doi:10.1002/2013JE004469.
- 738 Vaucher, J., D. Baratoux, N. Mangold, P. Pinet, K. Kurita, M. Gregoire, (2009) The volcanic  
739 history of central Elysium Planitia: Implications for Martian magmatism. *Icarus*, 204:  
740 418-422.
- 741 Vetterlein, J. and Roberts, G. P. (2009) Postdating of flow in Athabasca Valles by faulting  
742 of the Cerberus Fossae, Elysium Planitia, Mars. *Journal of Geophysics Research*.
- 743 Vetterlein, J. and Roberts, G. P. (2010) Structural Evolution of the Northern Cerberus  
744 Fossae graben system, Elysium Planitia, Mars. *Journal of Structural Geology*, 32:  
745 394-406.
- 746 Wells, D. L. and Coppersmith, K. J. (1994) New empirical relationships among magnitude,  
747 rupture length, rupture width, rupture area, and surface displacement. *Bulletin of the*  
748 *Seismological Society of America*, 84, (4): 974-1002.

749

## 750 **Figure Captions**

751

752 **Figure 1.** Hypotheses to explain the characteristics of the widest examples of boulder  
753 trails formed by the mobilised boulder populations due to seismic shaking and release of  
754 boulders from cliffs by melting of ice. (a) Alternative hypotheses explored by Roberts et al.  
755 (2012). (b) Terrestrial rockfalls triggered by an earthquake. (c) Data from Roberts et al.  
756 (2012) for comparison with data presented in this paper.

757

758 **Figure 2.** Location maps. (a) MOLA images of Mars showing the location of the study  
759 area. (b) NASA image mosaic (visible imagery) with the location of the study area shown.  
760 The four white squares show the locations of the four geological and geomorphological  
761 interpretations for Images 1, 3, 9 and 12 (see Figure 4 (a), (b), (c) & (d)). (c) Map showing  
762 location of the studied boulder trail anomalies. Boulder Trail Anomaly 1 (red) and Boulder  
763 Trail Anomaly 2 (green) and location of HiRISE image footprints across the study area,  
764 numbered in accordance with number scheme used in this study. HiRISE images 1  
765 through 13 were used in this study. (d) and (e) show details of the fault geometries and  
766 geomorphology and are located in (c) .

767

768 **Figure 3. (a)** Images showing typical locations and attributes of the boulder trails counted  
769 in this study. **(b) and (c)** A selection of images showing the variation in boulder trails  
770 between different HiRISE images and different parts of the same HiRISE images. (i)  
771 original image, with added white arrows pointing out a selection of boulder trails/bounce  
772 marks; (ii) the image with the boulder trail/bounce marks drawn in black, and (iii) with only  
773 the black infill. The figures illustrate only a small proportion of the total number of boulder  
774 trails in each image. **(d)** Observations of boulder trails and boulder dimensions. The  
775 similarity between the dimensions of boulders and boulder trails suggest that boulder trails  
776 have not been significantly affected by erosion.

777 (i) A possible hypothesis is that boulder trails may be degraded by erosion, and that  
778 degradation may vary spatially, influencing the number of trails that are preserved, and the  
779 widths that are measured. (ii) and (iii) Comparison of boulder trail widths with the  
780 dimensions of the boulders that formed them from ESP\_026712\_1960 and from  
781 ESP\_025156\_1965). (iv) Location map showing the position of ESP\_026712\_1960 and  
782 ESP\_025156\_1965. (v) That the trails have not been significantly degraded by wind  
783 erosion is consistent with the preservation of raised levees produced by the motion of  
784 boulders, evidenced by variation in percentage grayscale for individual pixels in the  
785 images. This is evidenced by visual inspection of many examples, and also evidenced by  
786 the percentage grayscale measurements we have made that show systematic variation in  
787 percentage grayscale on the floors of the tracks, not constant values as would be  
788 expected for a flat, depositional surface illuminated by the sun. If the levees are made of  
789 sand, and their preservation potential is low, then the ages of the boulder trails whose  
790 widths are defined by the levees is likely to be similar, and relatively young. In other words,  
791 the widespread preservation of levee crests in the images suggests the boulder trails are  
792 similar in age, because they have not been eroded/degraded. And that is what we use to  
793 suggest the population of boulder trails is mostly composed of individual trails of similar  
794 age, hence possibly produced in single, widespread events, that is, marsquakes.

795

796 **Figure 4. (a), (b), (c) & (d)** Geological and geomorphological interpretations of Images 1,  
797 3, 9 and 12. The geology/geomorphology on the fossae is that of a low-relief plain that has  
798 been faulted by graben structures, down-dropping central blocks that have been covered  
799 by colluvium and aeolian material.

800

801 **Figure 5.** The relationship between the map trace of the graben and vertical offsets  
802 constrained by MOLA data. **(a)** Plot of longitude against vertical offset measured across  
803 the south side of the graben from MOLA data. **(b)** CTX mosaic showing how the vertical  
804 offsets in (a) relate to the map geometry of the graben. **(c)** The location of MOLA data in  
805 latitude and longitude, showing how the vertical offsets in (a) relate to the map geometry of  
806 the graben. **(d)** Plot showing absolute values of elevation for the plain to the south of the  
807 graben, the plain north of the graben, and the floor of the graben, versus longitude.

808

809 **Figure 6.** Example of a boulder trail density measurement for two images: **(a)** Image 4  
810 (HiRISE Image ESP\_025011\_1965) and **(b)** Image 8 (HiRISE Image ESP\_026712\_1960).  
811 **(a).** Image 4 **(a. (i))** shows a sparse concentration of narrow trails, all of similar width and  
812 similar length. **a. (ii)** Blue dots at the apex of the dark lines indicate boulder trails along a  
813 transect shown in dark blue. **a. (iii)** Graph showing location and density of boulder trails  
814 found along a WNW-WSE transect traversing  $0.03^\circ$  of longitude, showing the locations of  
815 trails. **(b).** Image 8 **(b. (i))** shows a dense concentration of both narrow and some wider  
816 trails. The lengths of the trails in the image are comparable. Some trails exhibit bounce  
817 marks. **b. (ii)** Dots at the apex of the dark lines indicate boulder trails along a transect  
818 shown in dark blue. **b. (iii)** Graph showing location and density of boulder trails found  
819 along a WNW-WSE transect traversing  $0.05^\circ$  of longitude, showing the locations of trails.

820

821 **Figure 7.** Both authors counted boulder trails and boulder widths along Boulder Trail  
822 Anomaly 1 and Boulder Trail Anomaly 2. **(a)** Calibration graph for boulder trail counts. **(b)**  
823 Calibration graph for boulder width counts. Both of these results show that the results are  
824 repeatable with results from the two surveys being broadly comparable.

825

826 **Figure 8.** **(a)** Plot showing absolute values of elevation for the plain to the south of the  
827 graben, the plain north of the graben, and the floor of the graben, versus longitude. **(b)**  
828 Graph of longitude versus boulder trails per kilometer. **(c)** Graph of longitude versus  
829 boulder trails widths.

830

831 **Figure 9.** **(a)** Comparison of three data sets of boulder trails per kilometer against  
832 longitude for Boulder Trail Anomaly 1, Boulder Trail Anomaly 2 and data from Cerberus  
833 Fossae (Roberts et al. (2012)). Roberts et al. (2012) suggested that if the along strike  
834 extent of seismic shaking great enough to mobilize boulders on Earth is approximately the  
835 same as the along strike extent of surface faulting for the earthquake ruptures, it may be

836 possible to infer the magnitude of seismic events. Following this, if the long strike extent of  
837 the hump-shaped anomalies in boulder trail data are taken as proxies for along strike  
838 rupture extent, the implied moment magnitudes for the palaeomarsquakes, assuming that  
839 the humps result from single events, is in the range of Mw 7.3-7.8. **(b)** Comparison of three  
840 data sets of boulder trail density per kilometer against longitude for Boulder Trail Anomaly  
841 1, Boulder Trail Anomaly 2 and data from Cerberus Fossae (Roberts et al. (2012)). **(c)**  
842 Comparison of three data sets of ten widest boulder trails per kilometer against longitude  
843 for Boulder Trail Anomaly 1, Boulder Trail Anomaly 2 and data from Cerberus Fossae  
844 (Roberts et al. (2012)). **(d)** Graph of surface rupture length versus moment magnitude  
845 adapted from Wells and Coppersmith (1994). If the long strike extent of the hump-shaped  
846 anomalies seen in Figure 9 a-c in boulder trail data are taken as proxies for along strike  
847 rupture extent, the implied moment magnitudes for the palaeomarsquakes, assuming that  
848 the humps result from single events, is in the range of Mw 7.3-7.8.

849

850 **Figure 10. (a)** Comparison of three data sets of the ten widest boulder trails against  
851 boulder trails per kilometer for Boulder Trail Anomaly 1, Boulder Trail Anomaly 2 and data  
852 from Cerberus Fossae (Roberts et al. (2012)). **(b)** Comparison of three data sets of the  
853 maximum number of boulder trails per kilometer against length of boulder trail anomaly for  
854 Boulder Trail Anomaly 1, Boulder Trail Anomaly 2 and data from Cerberus Fossae  
855 (Roberts et al. (2012)). Note the positive correlation between the along strike length of the  
856 boulder trail anomaly and the maximum value for boulder trails per km recorded. This may  
857 be interpreted to suggest that maximum ground acceleration may increase with  
858 earthquake magnitude.

859

860 **Table1 HiRISE image observations used.**

861

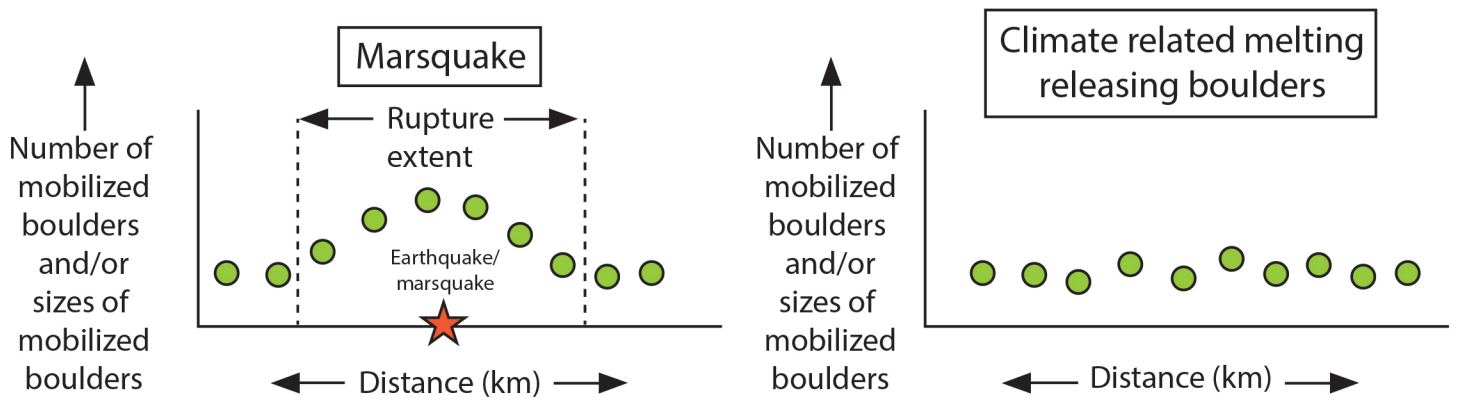
Image number used in this paper	HiRISE Image Name	Latitude (centered)	Longitude (East)	Map Projected Scale
1	PSP_008502_1965	16.250°	160.575°	25 cm / pixel
2	ESP_018774_1965	16.085°	160.723°	50 cm / pixel
3	PSP_006999_1965	16.100°	160.828°	25 cm / pixel
4	ESP_025011_1965	16.141°	161.011°	25 cm / pixel
5	ESP_018708_1960	15.819°	161.448°	50 cm / pixel
6a	ESP_027345	15.571°	161.792°	50 cm /

	_1955			pixel
<b>6b</b>	ESP_027345 _1955	15.571°	161.792°	50 cm / pixel
<b>8</b>	ESP_026712 _1960	15.715°	162.013°	25 cm / pixel
<b>9</b>	PSP_006287 _1955	15.479°	162.677°	25 cm / pixel
<b>10</b>	ESP_018075 _1955	15.386°	162.928°	25 cm / pixel
<b>11</b>	ESP_028400 _1955	15.329°	163.242°	25 cm / pixel
<b>12</b>	PSP_010361 _1955	15.311°	163.336°	25 cm / pixel
<b>13</b>	PSP_007790 _1955	15.209°	163.657°	25 cm / pixel

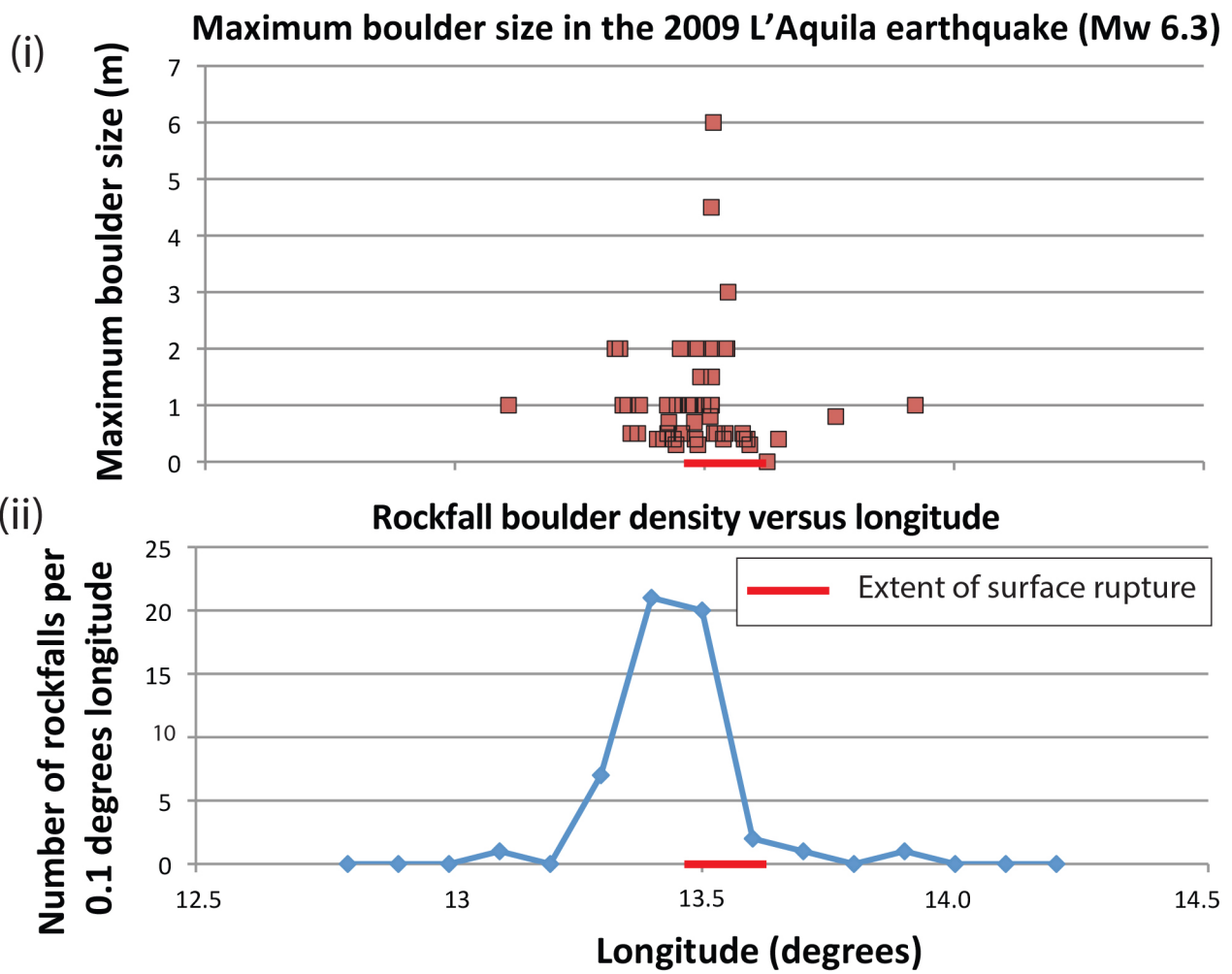


Figure 1

a) Hypothesis



b) Terrestrial dataset - 2009 Mw 6.3 Earthquake, L'Aquila, Italy



c) Martian dataset - Cerberus Fossae, Roberts et al. (2012)

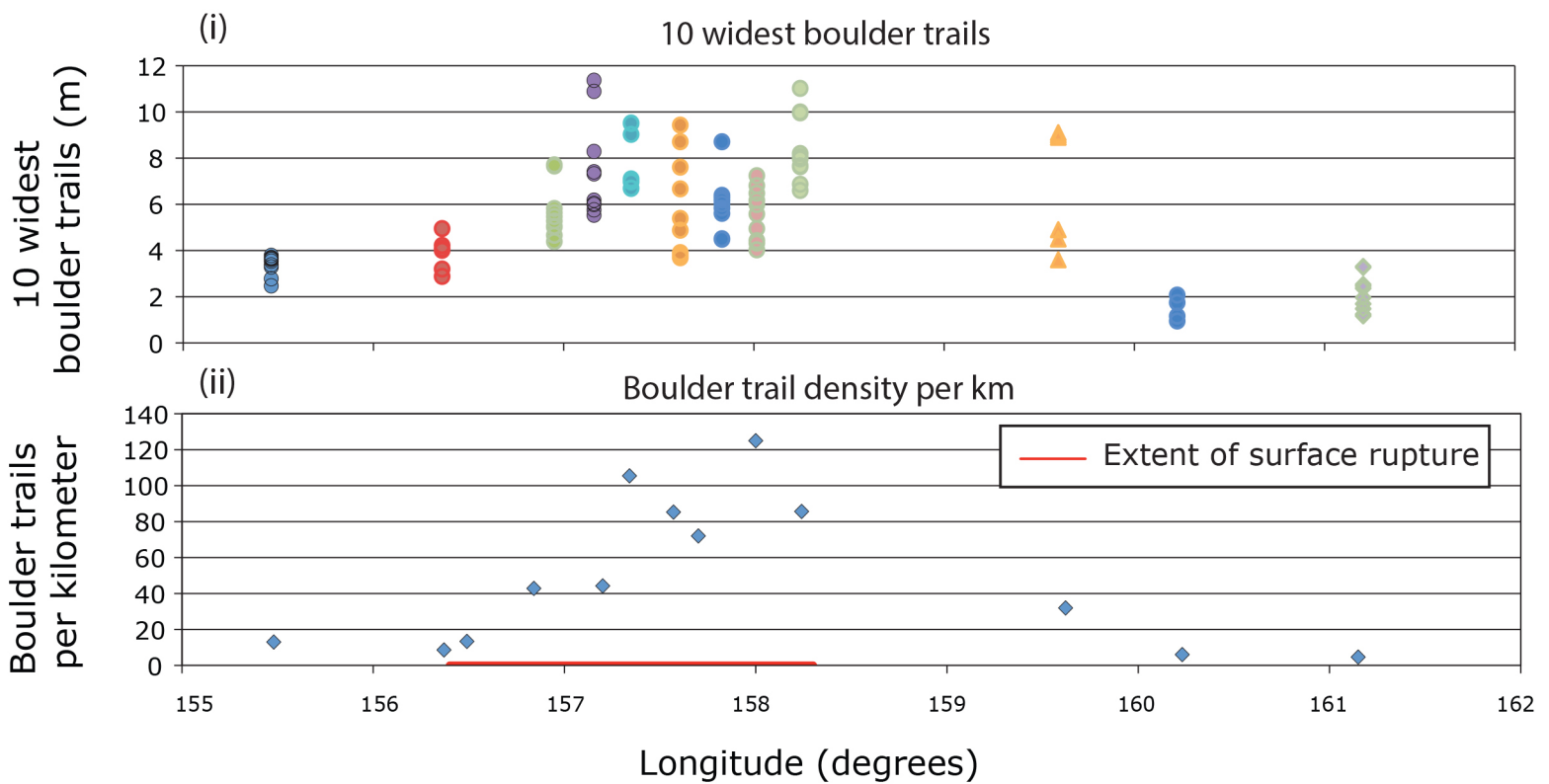
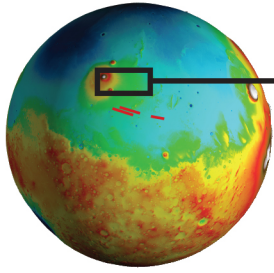
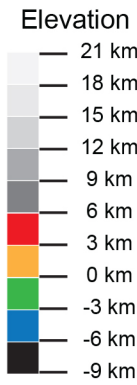
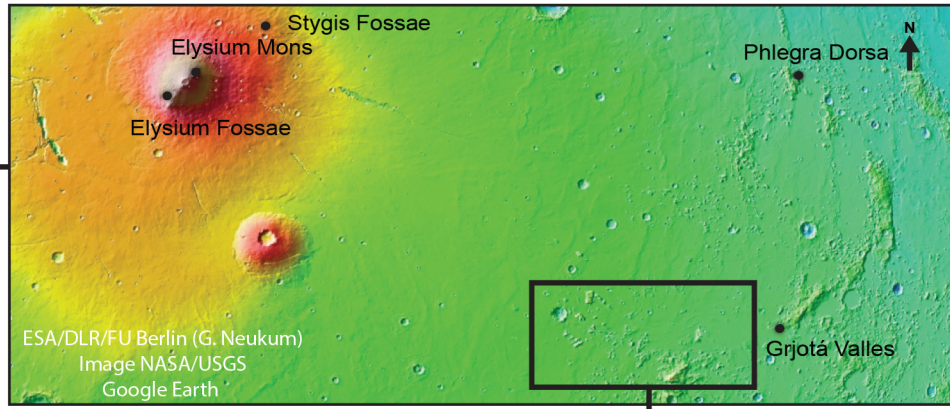


Figure 2

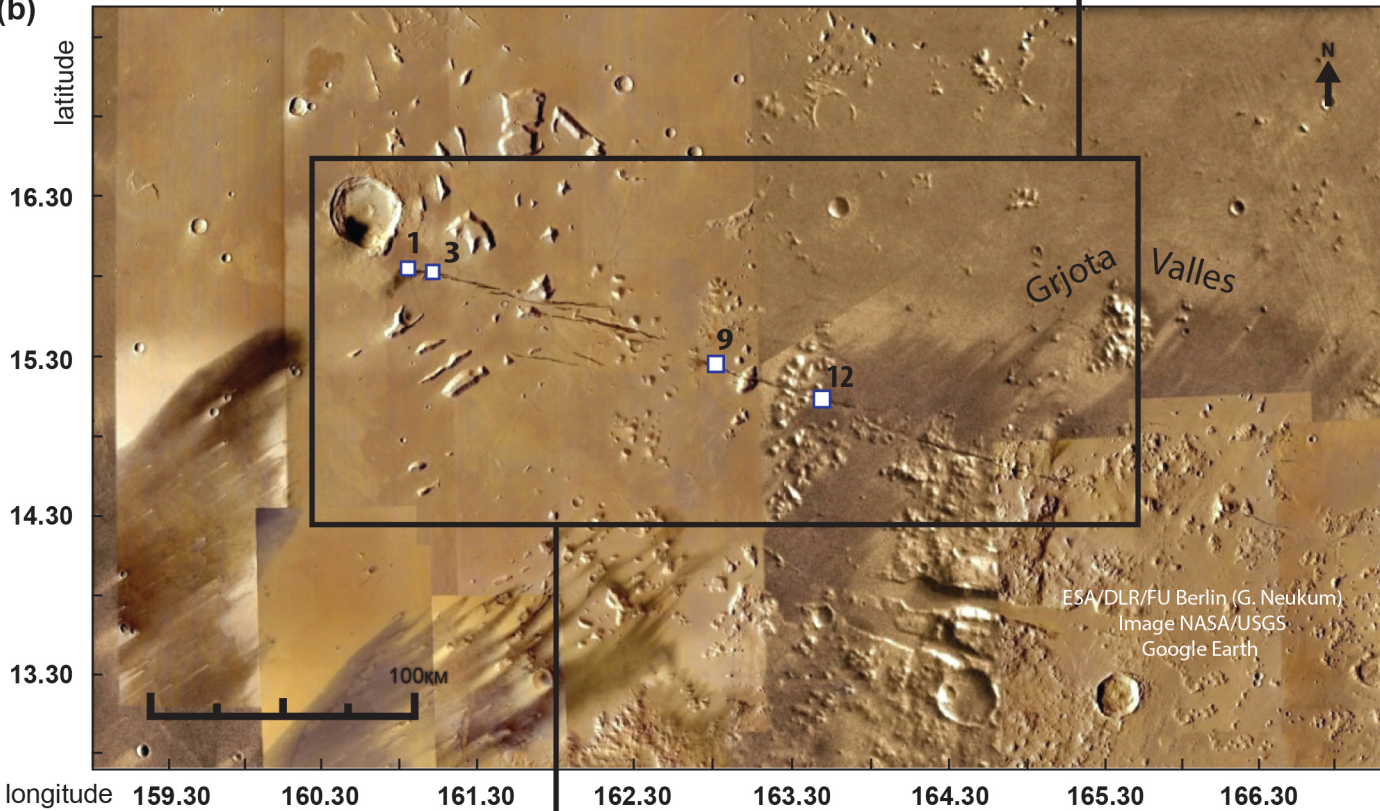
(a)



--- = Cerberus Fossae



(b)



(c)

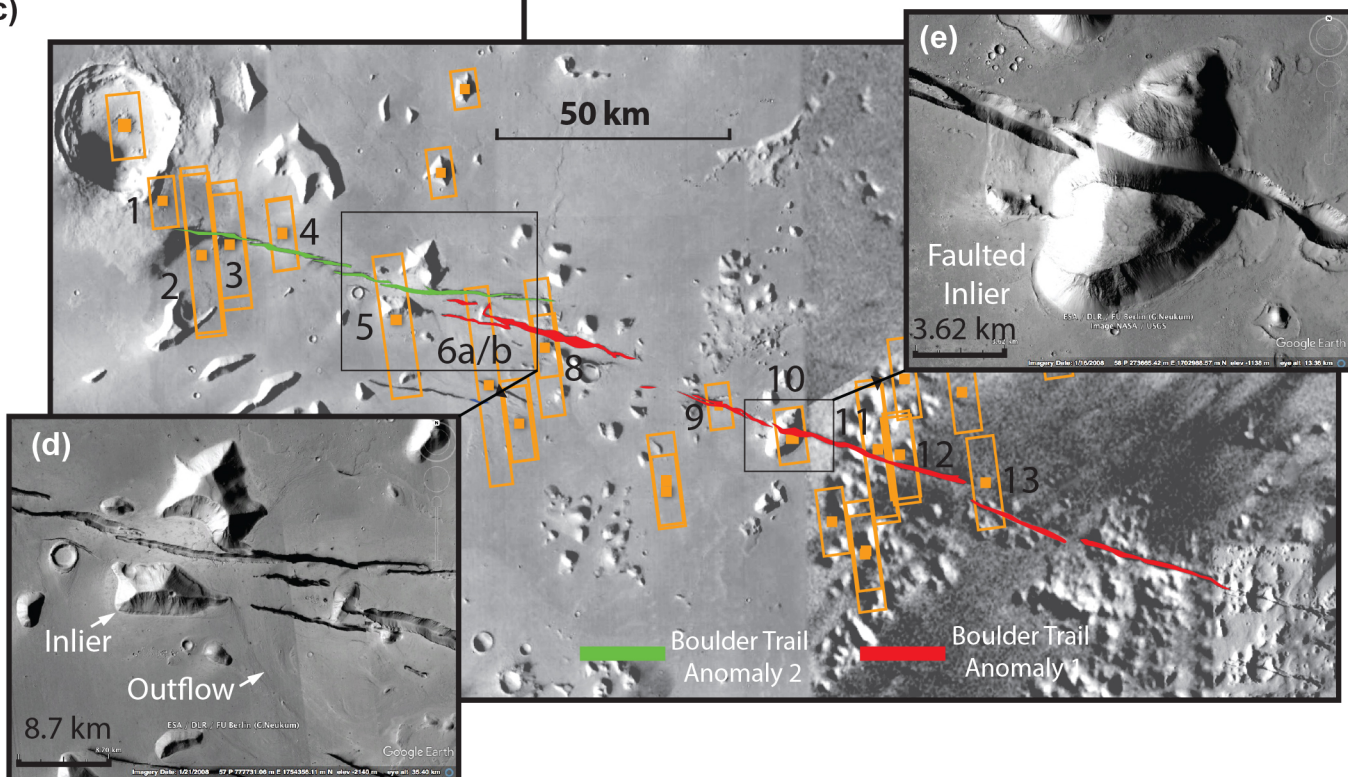
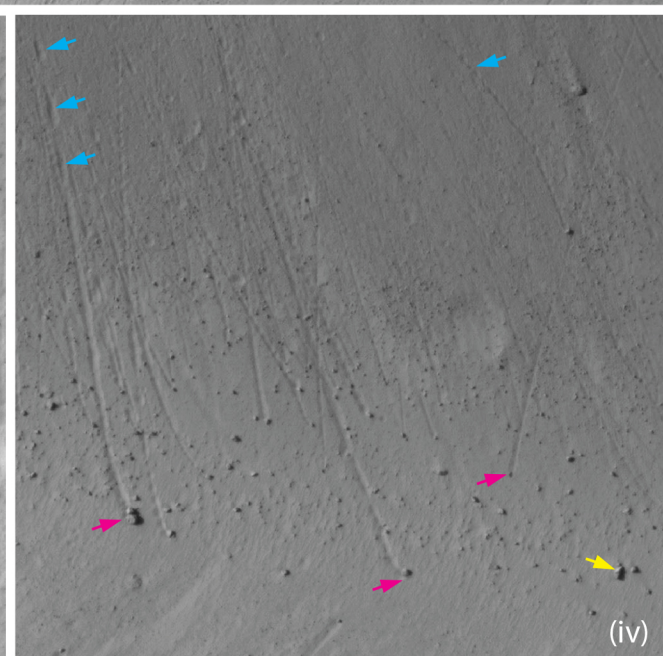
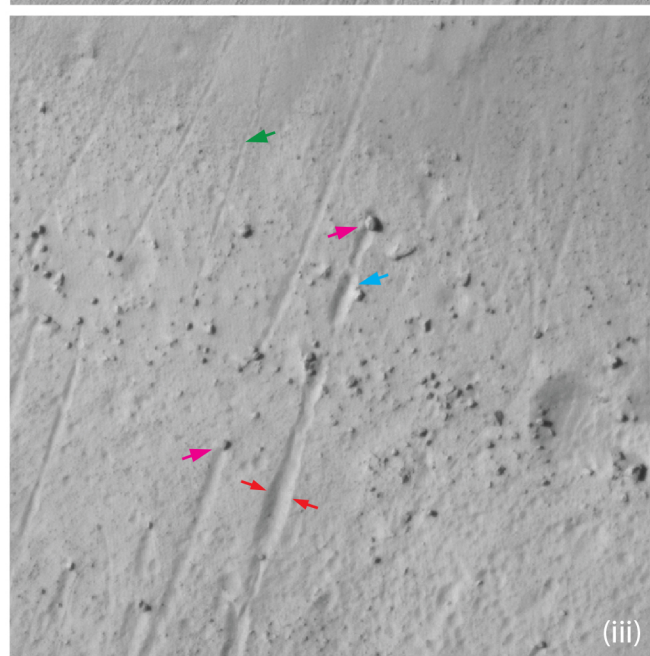
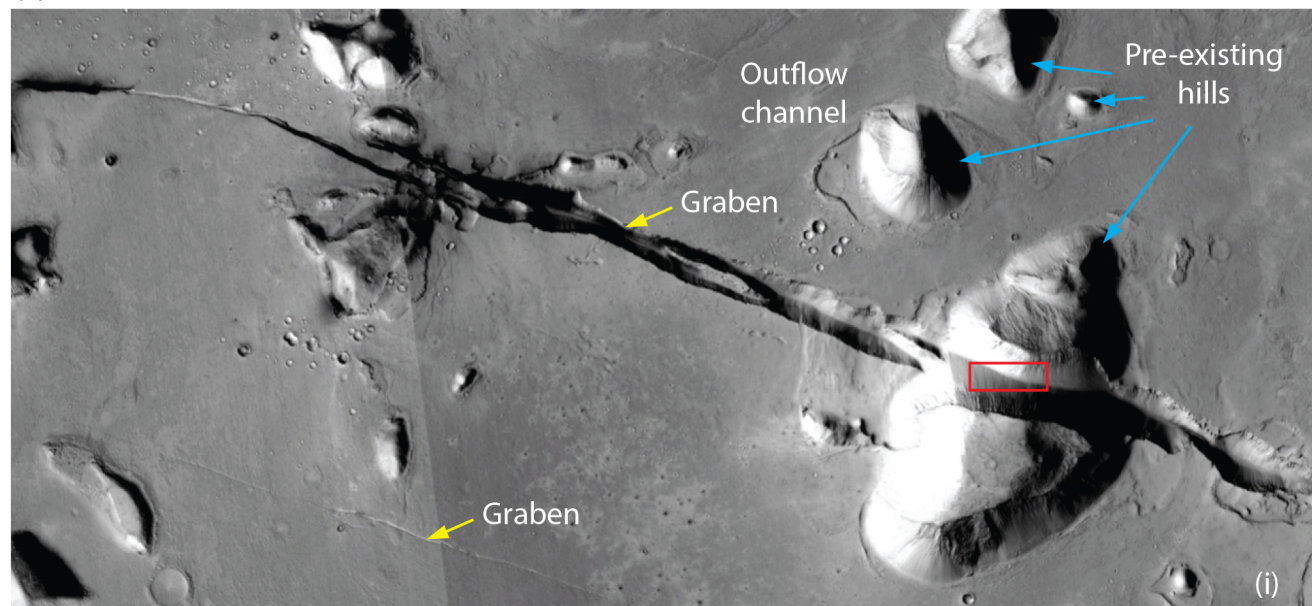




Figure 3

(a)








-  = Trail measured at widest point on trail defined by raised levees and sharp edges to trails
-  = elliptical depressions indicate bouncing
-  = boulder with no trail not included in count
-  = clear boulder that produced a trail
-  = trail with no clear boulder included in count



Figure 3 b (b)

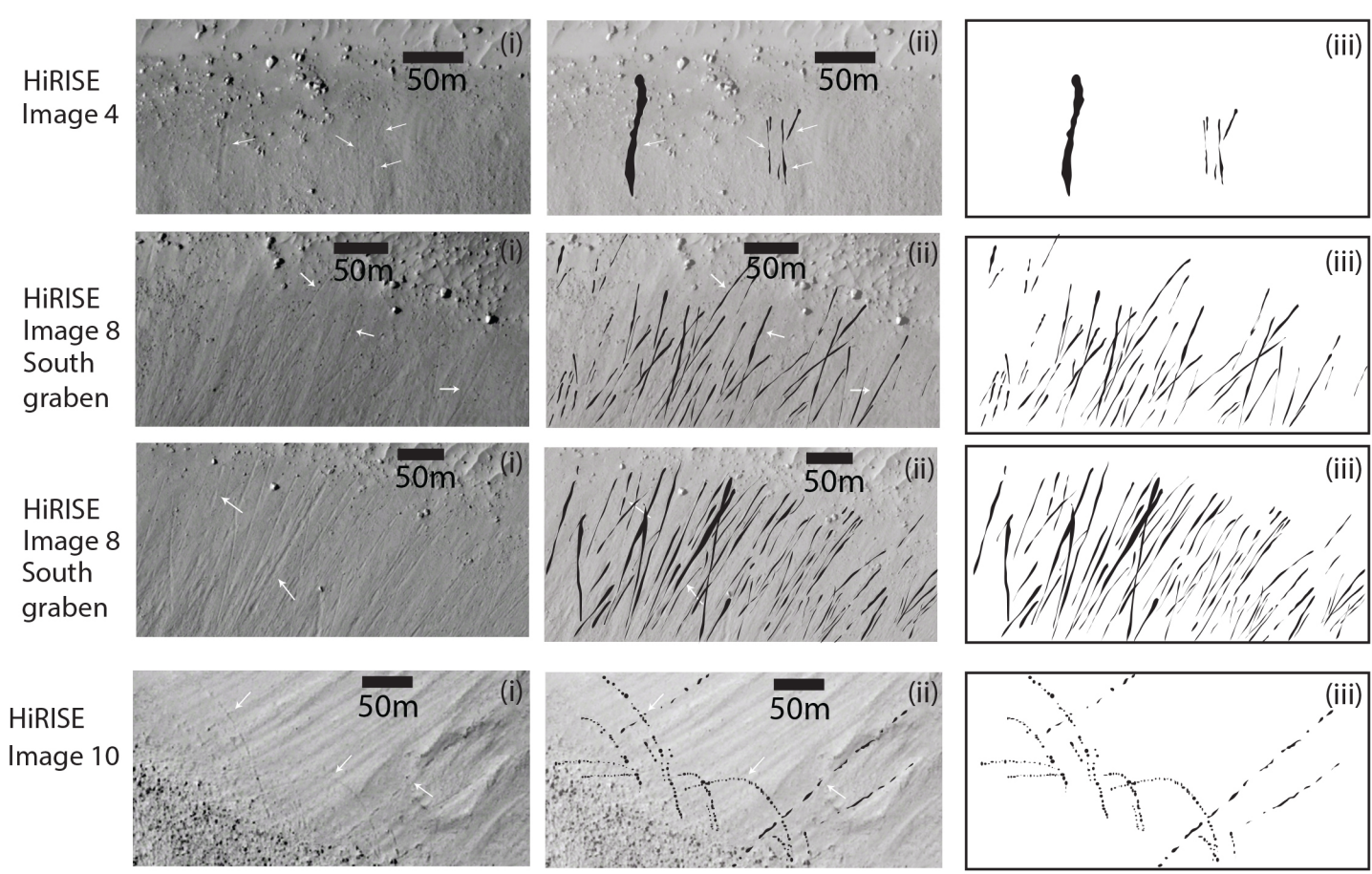
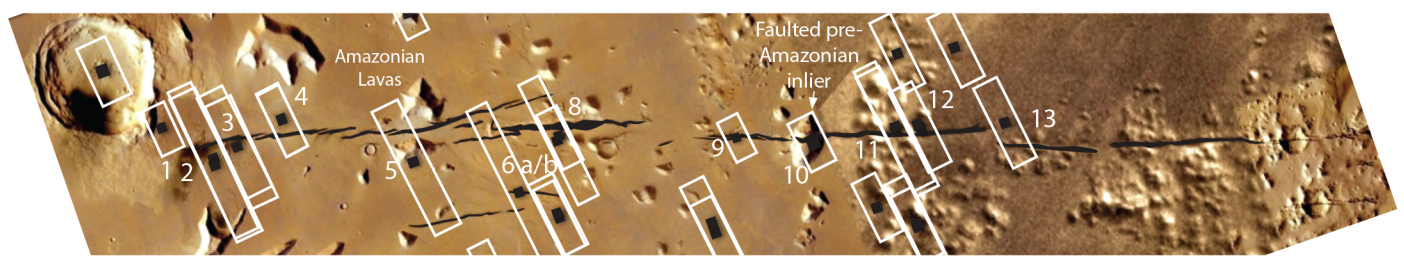
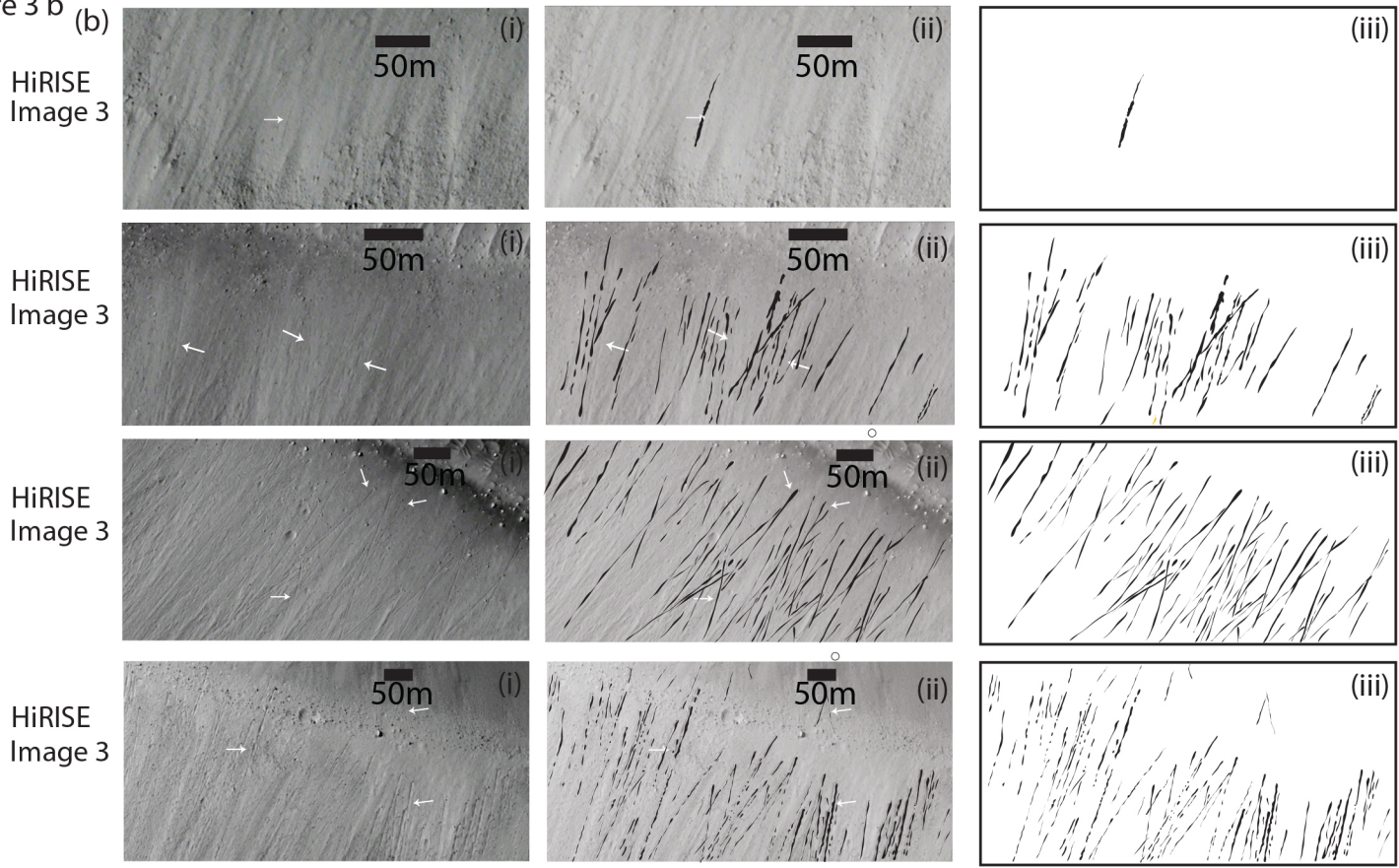




Figure 3 c

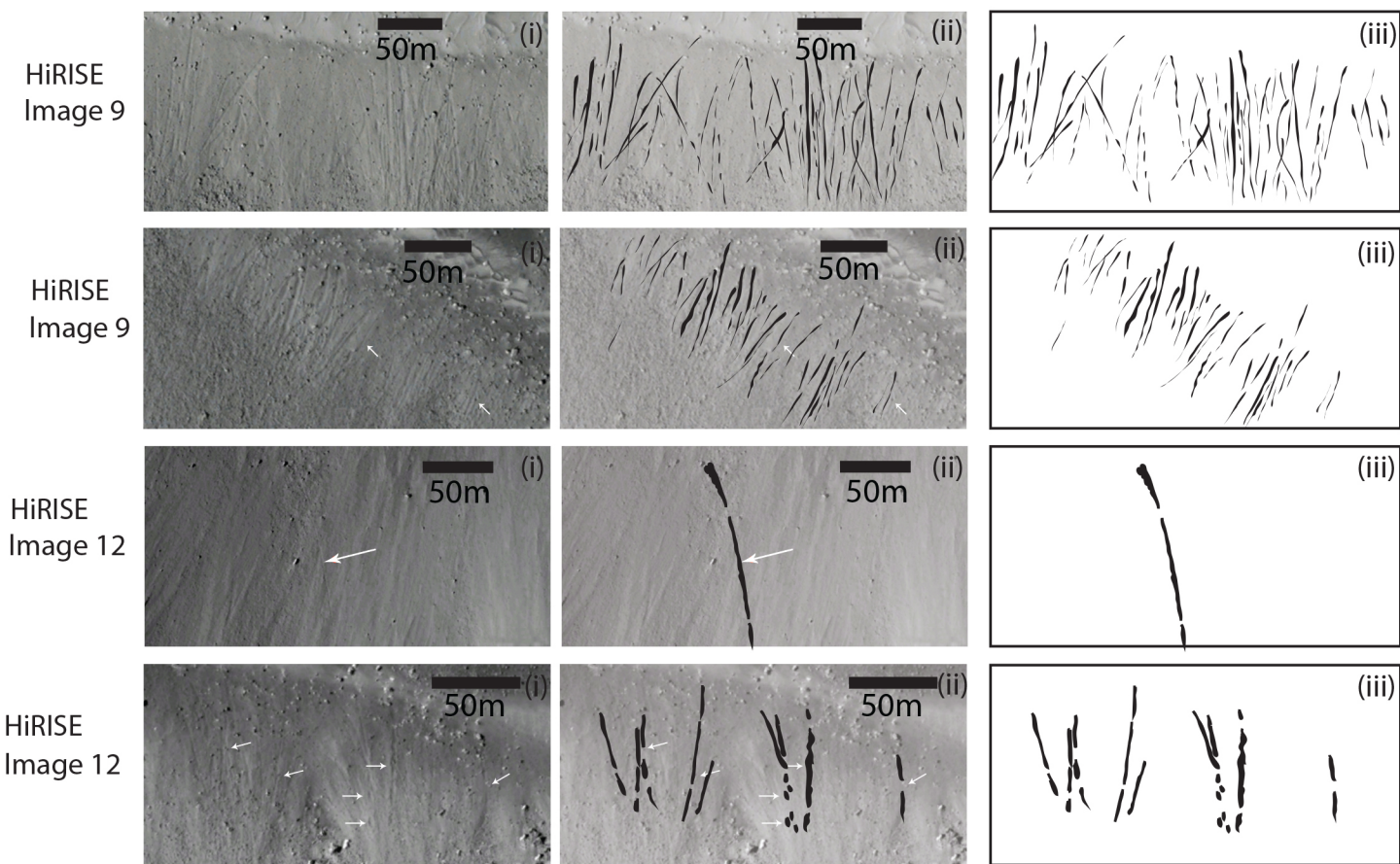
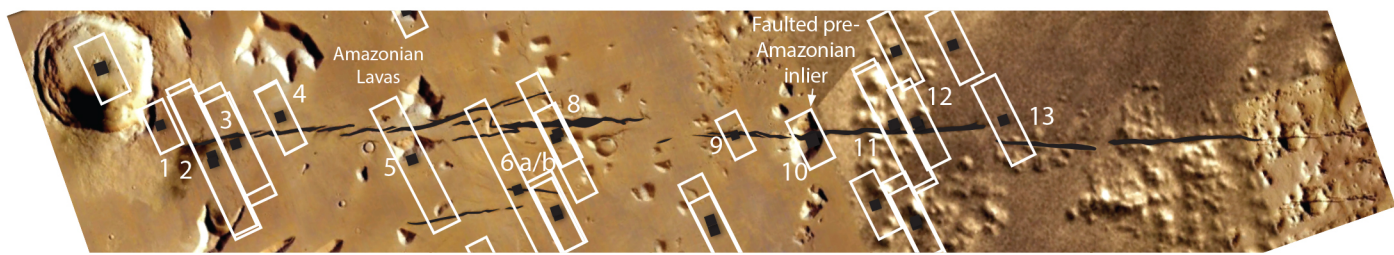
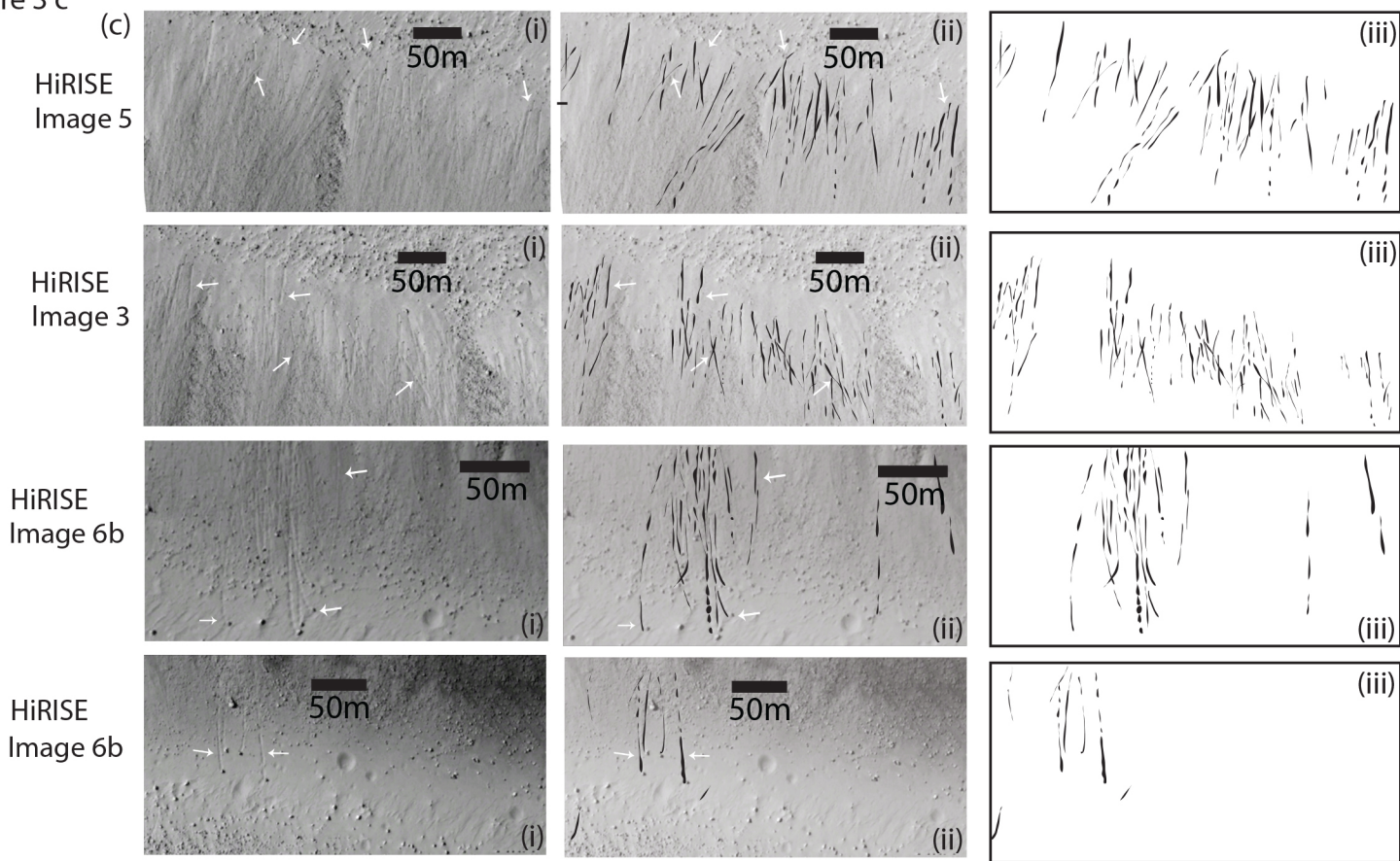
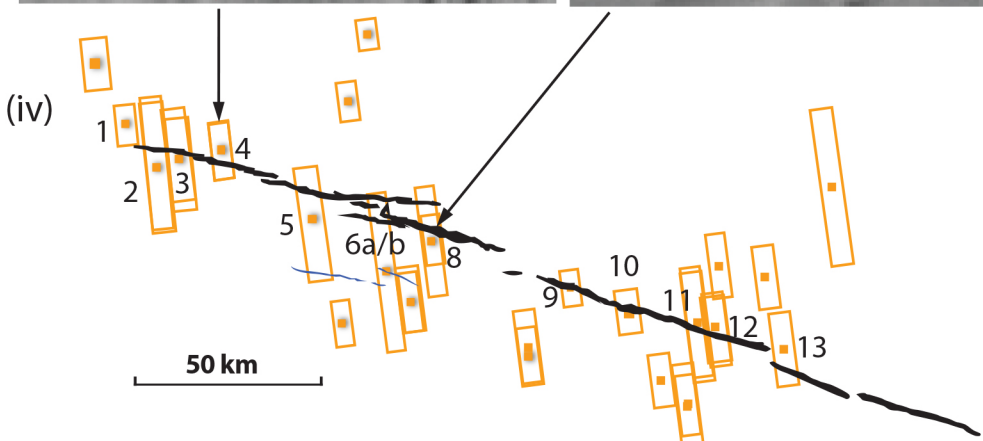
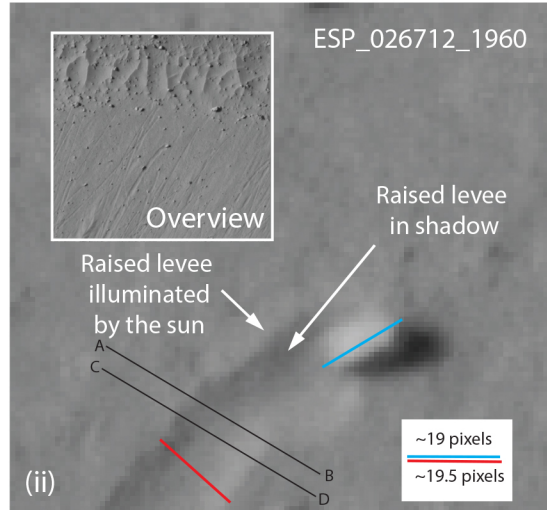
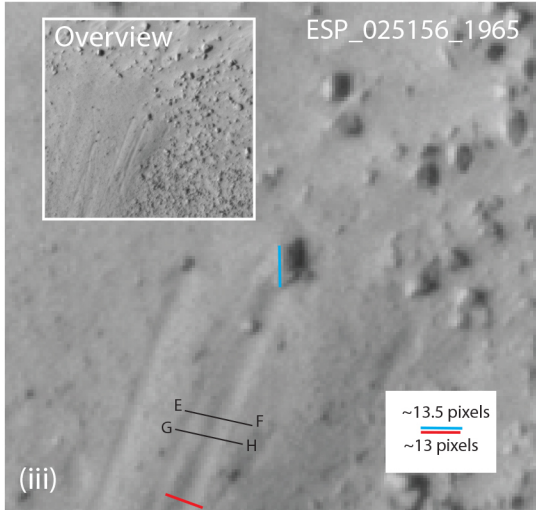
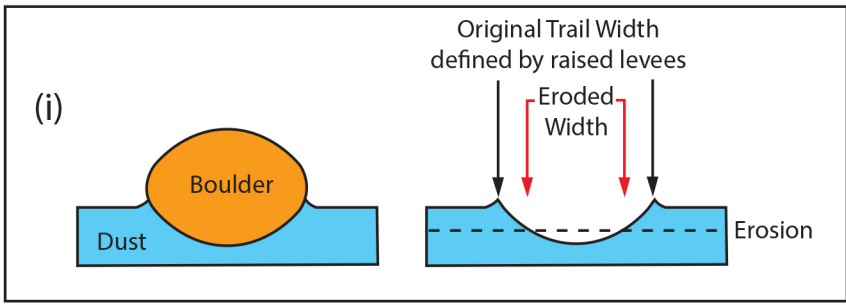
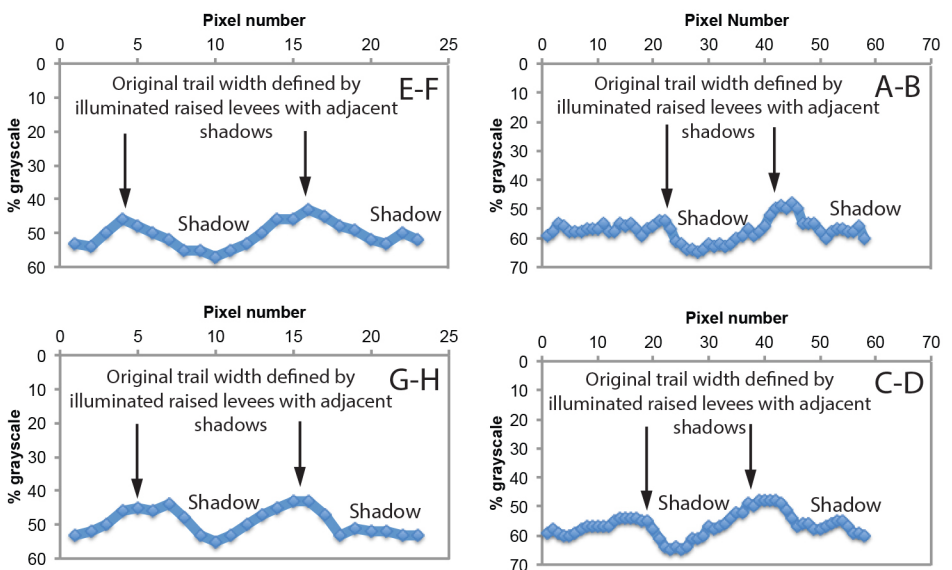


Figure 3 d



(v)

Distance versus % grayscale for individual pixels



Lower % grayscale values indicate raised, illuminated levees, with higher values indicating shadows produced by the levees







Figure 4 (a)







Image 1.

PSP\_008502\_1965 HIRISE IMAGE

N  
 Top right corner of image  
 16° 10' 14.80" N  
 160° 35' 24.20" E

Key:

- 10  Impact craters.
- 9  Scree slopes, predominately on the southern side of the depression.
- 8  Southern cliff/slope (dots denote presence of boulder). Colluvial deposits. Some bedrock lavas exposed?
- 7  Edge of northern cliff area with dark material forming cliff/slope face (dots denote presence of boulders). Colluvial deposits.

- 6  Mixed area of material from scree slopes and dunes.
- 5  Aeolian dunes (Transverse) of North to South orientation. Also, complex aeolian ripple structures (megaripple structures).
- 4  Lighter coloured areas found only in four locations outside the depression. Possibly terrain (1) that has been cleaned of dust.
- 3  Line marking the edge of the depression.
- 2  Smoother, less rugged terrain with aeolian dust deposits
- 1  Oldest Terrain. Rugged, upstanding ridges. Circular depressions indicate poorly-preserved craters. Cratered lava surface?

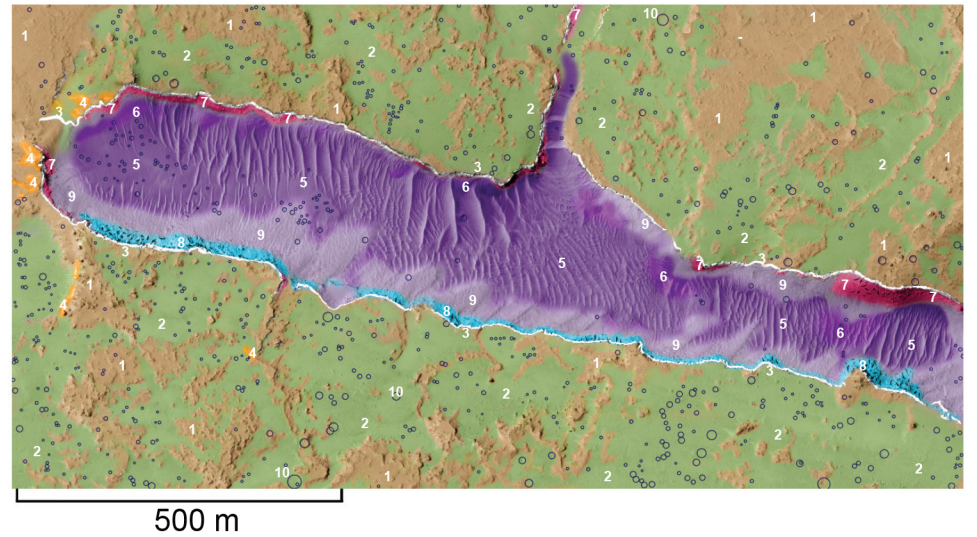
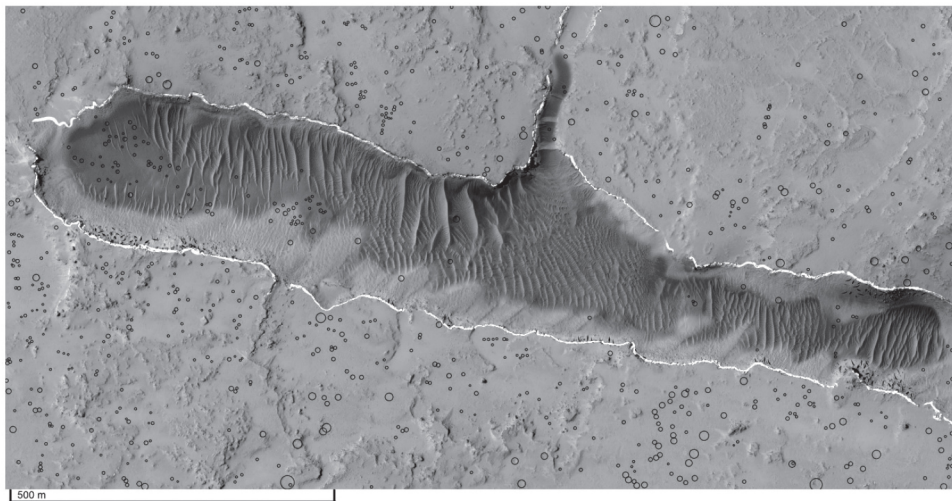





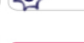







Figure 4 (b)













Image 3.

PSP\_006999\_1965 HIRISE IMAGE

N  
 Top right corner of image  
 16° 9' 27.66" N  
 160° 52' 41.96" E

Key:

- 23  Dunes
- 22  Denotes divide between coarser and finer grained areas.
- 21  Impact craters.
- 20  Impact crater with pedestal crater.
- 19  Inner edge of northern cliff area with dark material forming cliff slope face. The edge appears sharp and lacks boulders / debris.
- 18  Scree slope on southern side of depression.
- 17  Area denoting darker material found towards edge of depression (3 locations). May be a lava surface cleared of dust.
- 16  Defined slope face / cliff face along southern edge of depression, leading to rougher scree slopes down-slope. Some bedrock lava?
- 15  w / boulders / various sizes of metre-scale.
- 14  Aeolian dunes (Transverse) of North to South orientation. Also, complex aeolian ripple structures (megaripple structures).
- 13  Scree slopes, predominately on the southern side of the depression.

- 12  Denotes edge of depression area.
- 11  Possible edge of adjoining depression area.
- 10  Colluvial deposits. Coarse-grained / darker material.
- 9  Colluvial deposits. Coarser grained / darker material with evidence of aeolian influence (dune formations).
- 8  Colluvial deposits, that appear coarse-grained.
- 7  Denotes presence of boulders.
- 6  Fine grained aeolian dust/sand featuring megaripple structures/transverse dunes in NE→SW orientation + N→S orientation.
- 5  Complex dune patterns.
- 4  Oldest Terrain. Rugged, upstanding ridges. Circular depressions indicate poorly-preserved craters. Possibly a cratered lava surface.
- 3  Area to lower left of image appear to display an echelon form. (Also middle left image). Note: presence of aeolian dunes still visible in some higher rigged areas.
- 2  Mixture of rougher/coarser material, a with more rugged presence of aeolian transverse dunes. Mix of terrains (4), (5) and (6).
- 1  Outline of more obviously defined terrain (4).

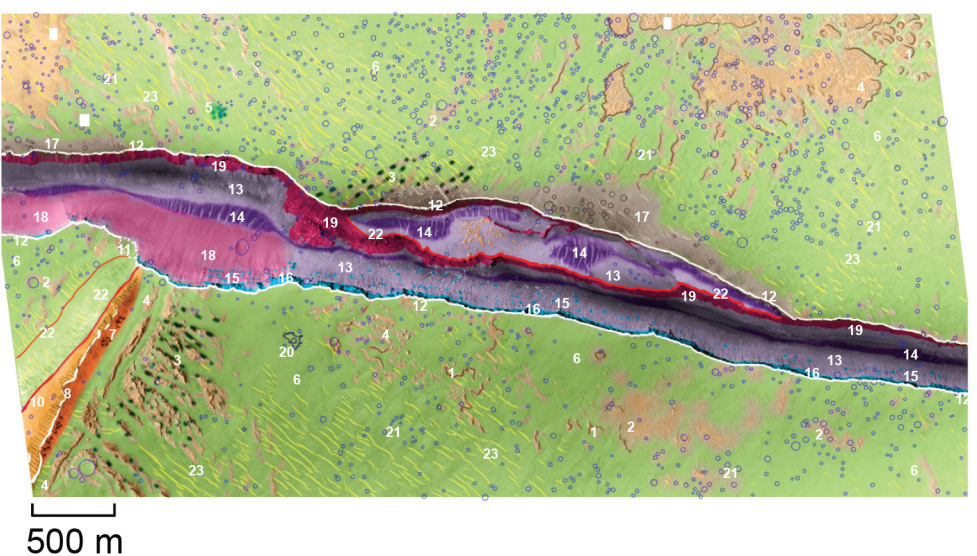
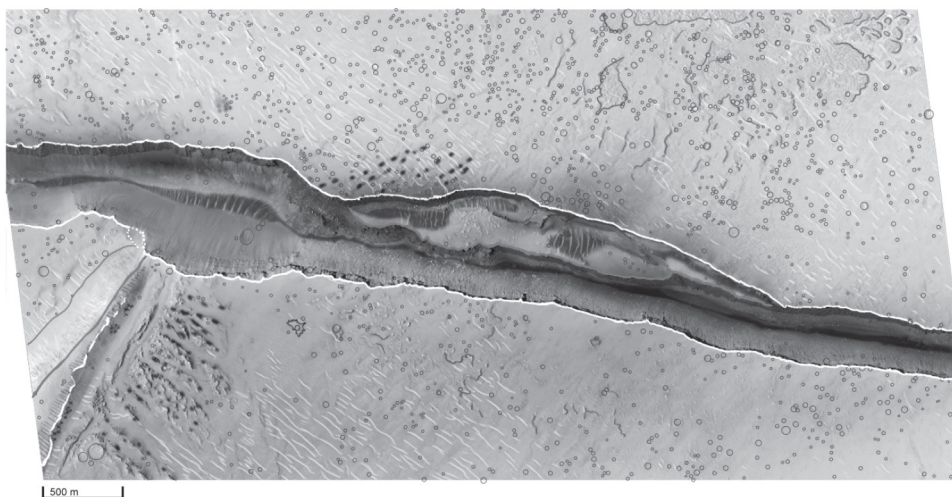















Figure 4 (c)

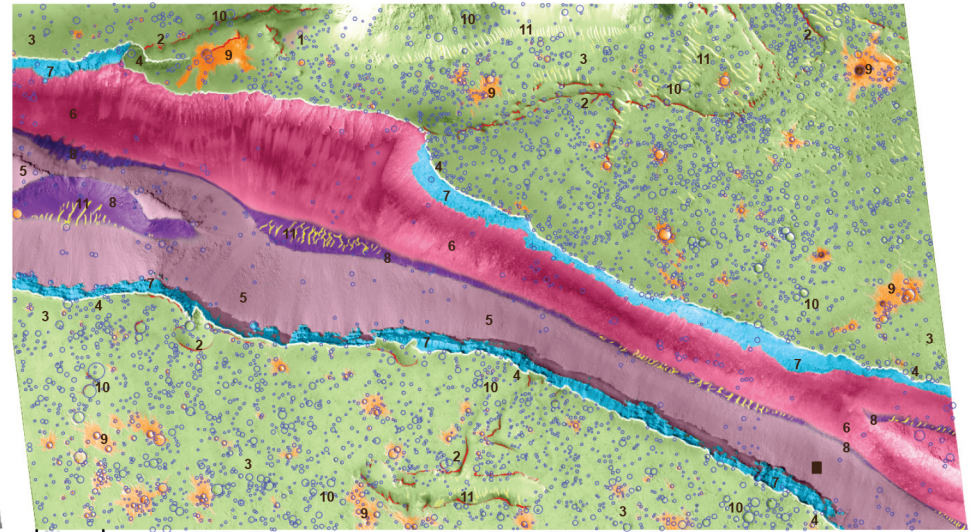
Image 9.  
PSP\_006287\_1955 HIRISE IMAGE

N  
↑ Top right corner of image  
15° 32' 6 • 85" N  
162° 44' 48 • 75" E

Key:

- 11  Dunes
- 10  Impact craters.
- 9  Impact craters with ejecta blankets.
- 8  Aeolian dunes/ripple structures on floor of depression.
- 7  Defined slope face/cliff face along parts of both the northern and southern edge of the depression. Bedrock lavas?

- 6  Colluvial deposits. Inner edge/slope of northern part of depression with dark material forming the cliff slope face.
- 5  Colluvial deposits. Inner edge/slope of southern part of depression with dark material forming the cliff slope face. Note the presence of fallen boulders from cliff face located towards the base of the depression.
- 4  Line denotes the edge of the depression.
- 3  Fine grained aeolian dust/sand pitted with impact craters.
- 2  Lines denote higher, ridged areas
- 1  Oldest Terrain. Rugged, up-standing ridges. Possibly a cratered lava surface.













500 m








Figure 4 (d)

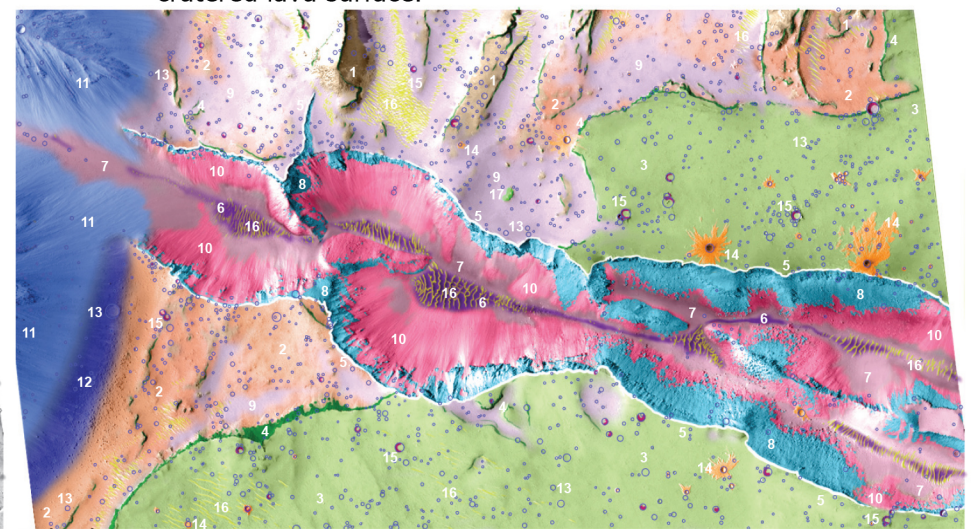
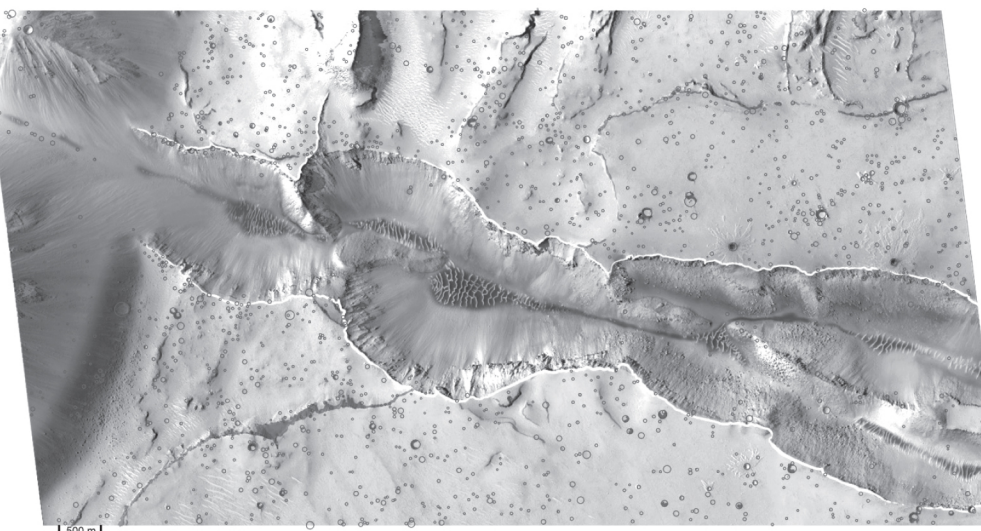
Image 12.  
PSP\_010361\_1955 HIRISE IMAGE

N  
↑ Top right corner of image  
15° 21' 3 • 11" N  
163° 25' 47 • 94" E

Key:

- 17  Unidentified Structure – Possible impact crater or ridge/upland area.
- 16  Aeolian Dunes – Present both in and out of the depression. These Aeolian dunes found in the depression form megaripple structures.
- 15  Impact craters with significant degradation, with some detail lacking, with eroded rims, eroded interiors, in-filled interiors.
- 14  Impact craters with ejecta blankets.
- 13  Impact craters.
- 12  Colluvial deposits.
- 11  Colluvial deposits lower on slope.
- 10  Inner edge/slope of depression, forming smooth and even scree slope.
- 9  A mix of terrain (7 and 10).
- 8  Defined slope face/cliff face along parts of both the north and south edge of the depression. Exposed bedrock (lavas?) with colluvial deposits lower on the slopes. Towards the east of the image, the defined slope face/cliff face descends down to the depression floor. Colluvium covered in boulders in places.

- 7  Colluvial deposits. Inner edge/slope of southern part of depression with dark material forming the cliff slope face – Note presence of fallen boulders from cliff face located towards foot of depression.
- 6  Aeolian dunes/ripple structures on floor of depression.
- 5  Denotes Edge of Depression.
- 4  Divide – Between two similar areas (fine grained aeolian areas). The line is demarked by presence of small boulders and a small difference in elevation between the two areas. Generally, the areas to the North and East of the line appear to be slightly lower in elevation, with the line marking a minor minor scree slope. Relative age of material either side of the divide difficult to discern. Dunes/impact craters are similar on both sides.
- 3  Fine Grained Aeolian dust/sand. Megaripple structures, impact craters and buried craters.
- 2  Fine Grained Aeolian Area of Lower Elevation than terrain (3). Similar to (7), but with a indistinct hummocky appearance. Predominates in southern region of image.
- 1  Oldest Terrain. Rugged, high-standing ridges. Possibly a cratered lava surface.



500 m



Figure 5

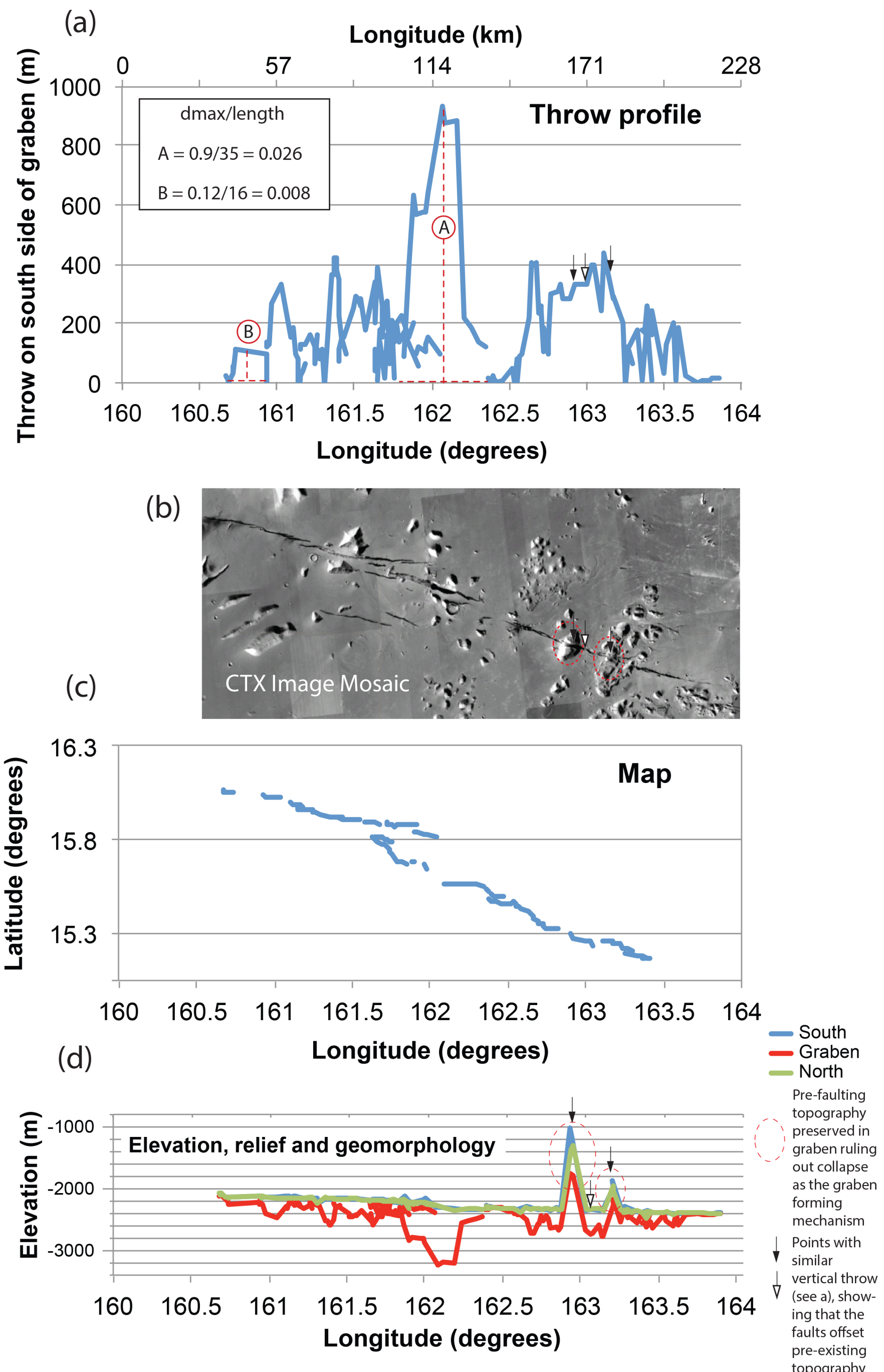


Figure 6

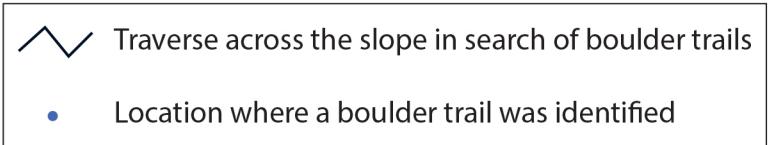
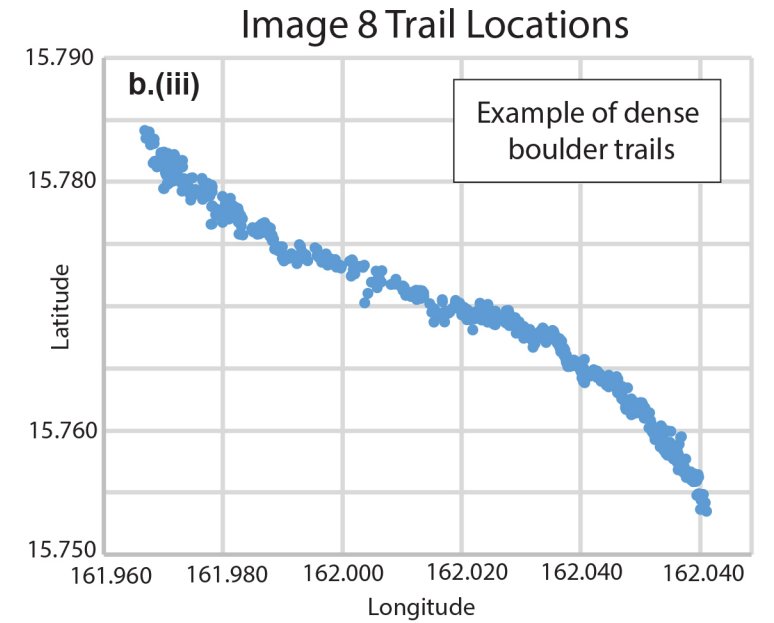
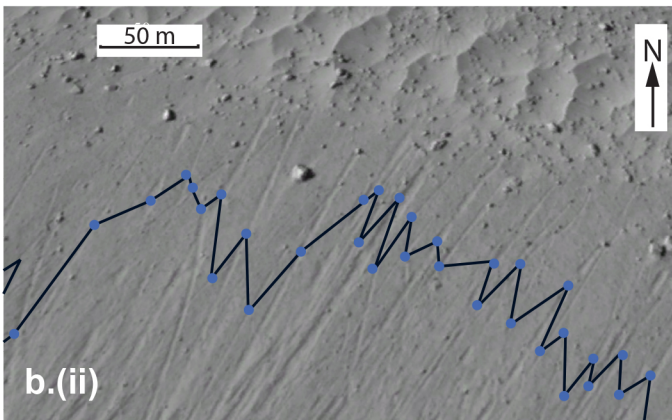
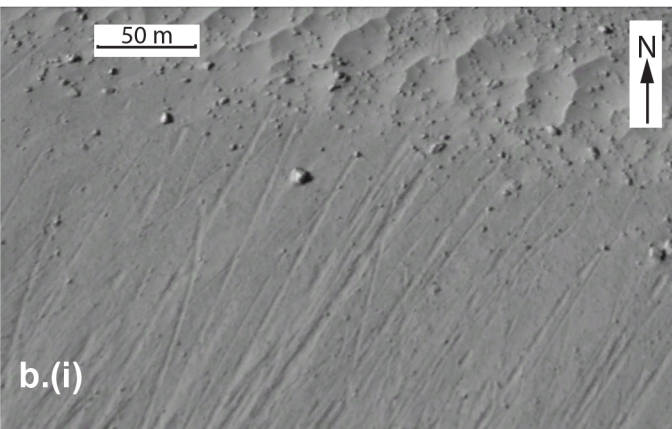
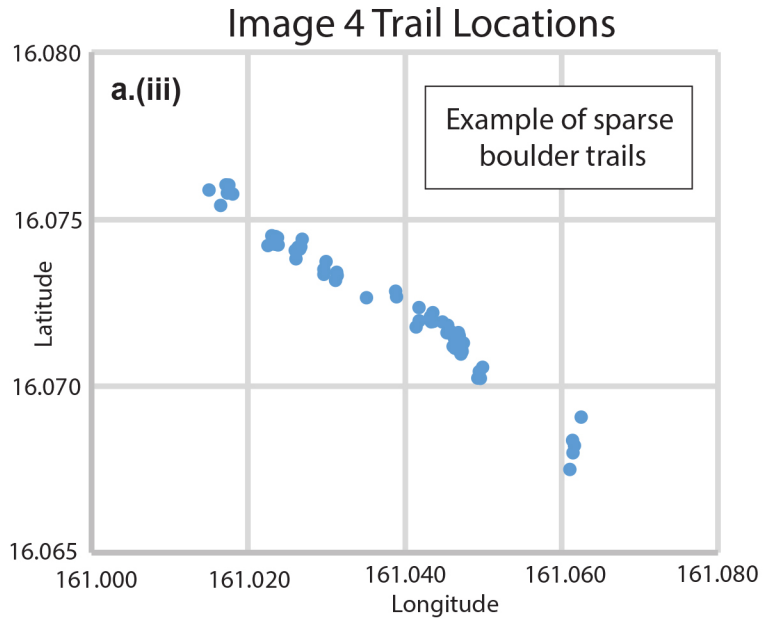
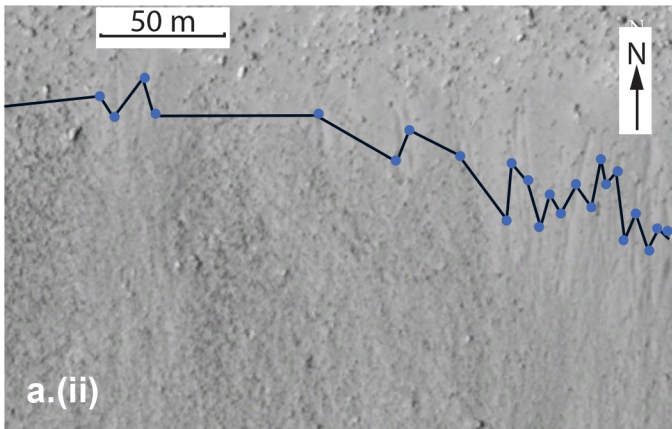
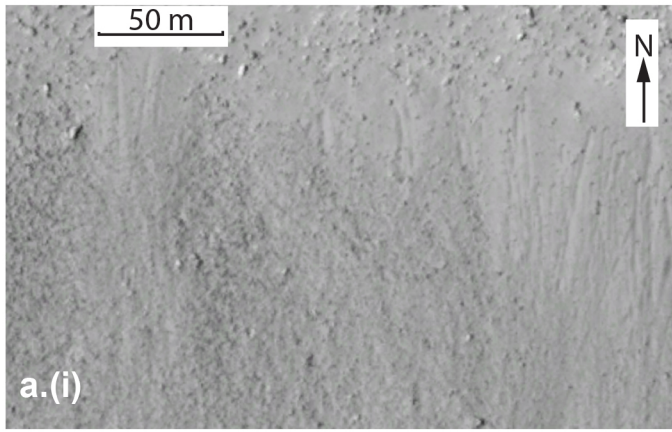
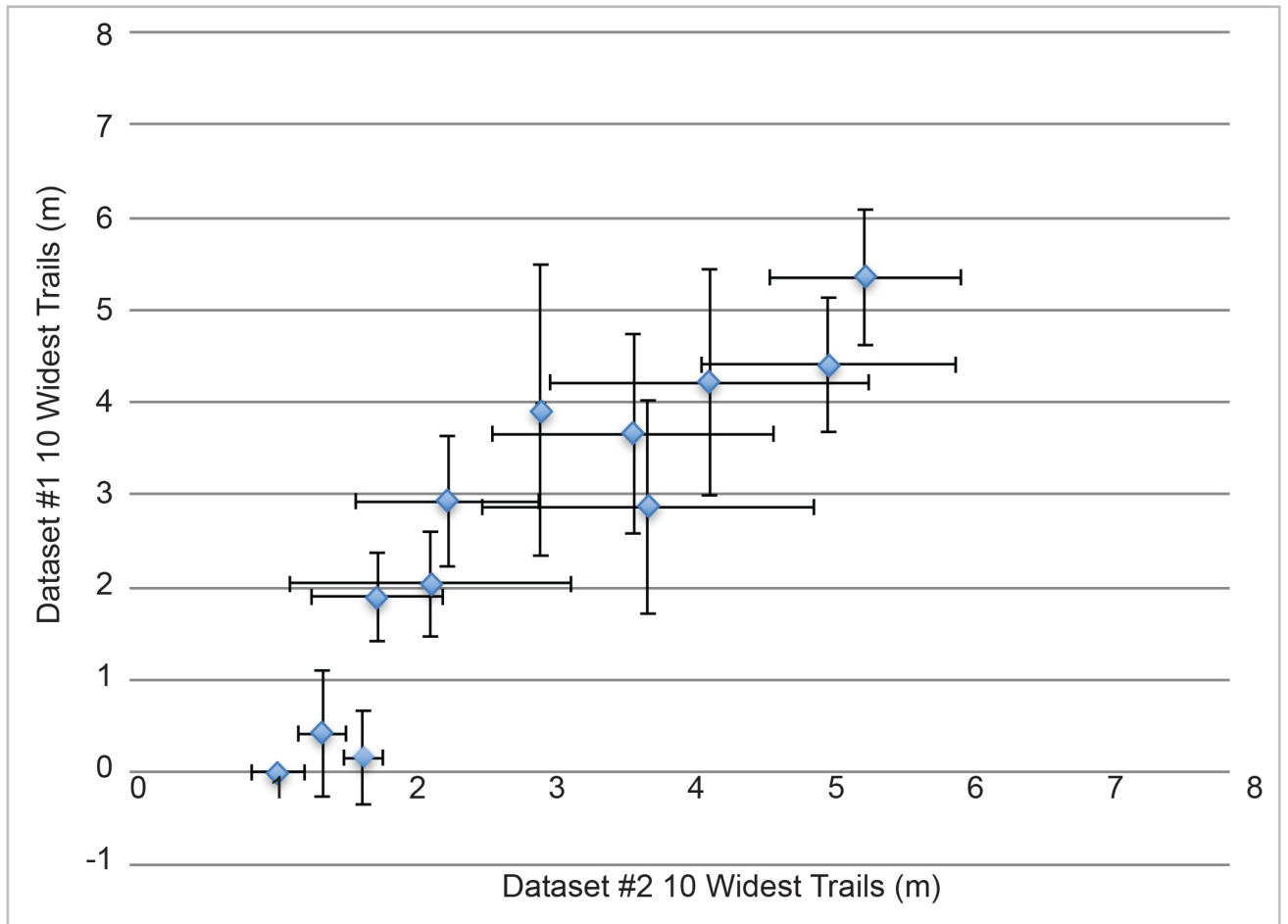


Figure 7

(a) Calibration - 10 Widest Trails



(b) Calibration - Boulder Trail Counts per Kilometre

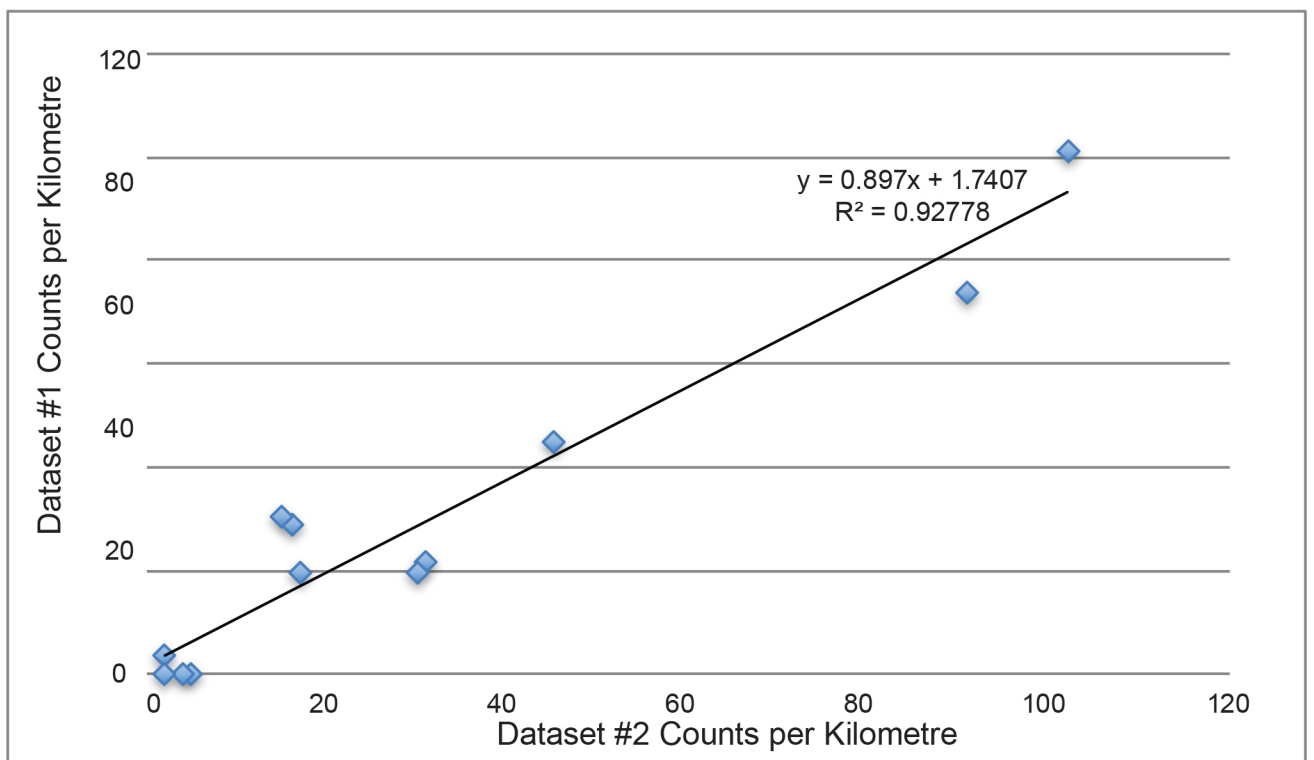


Figure 8

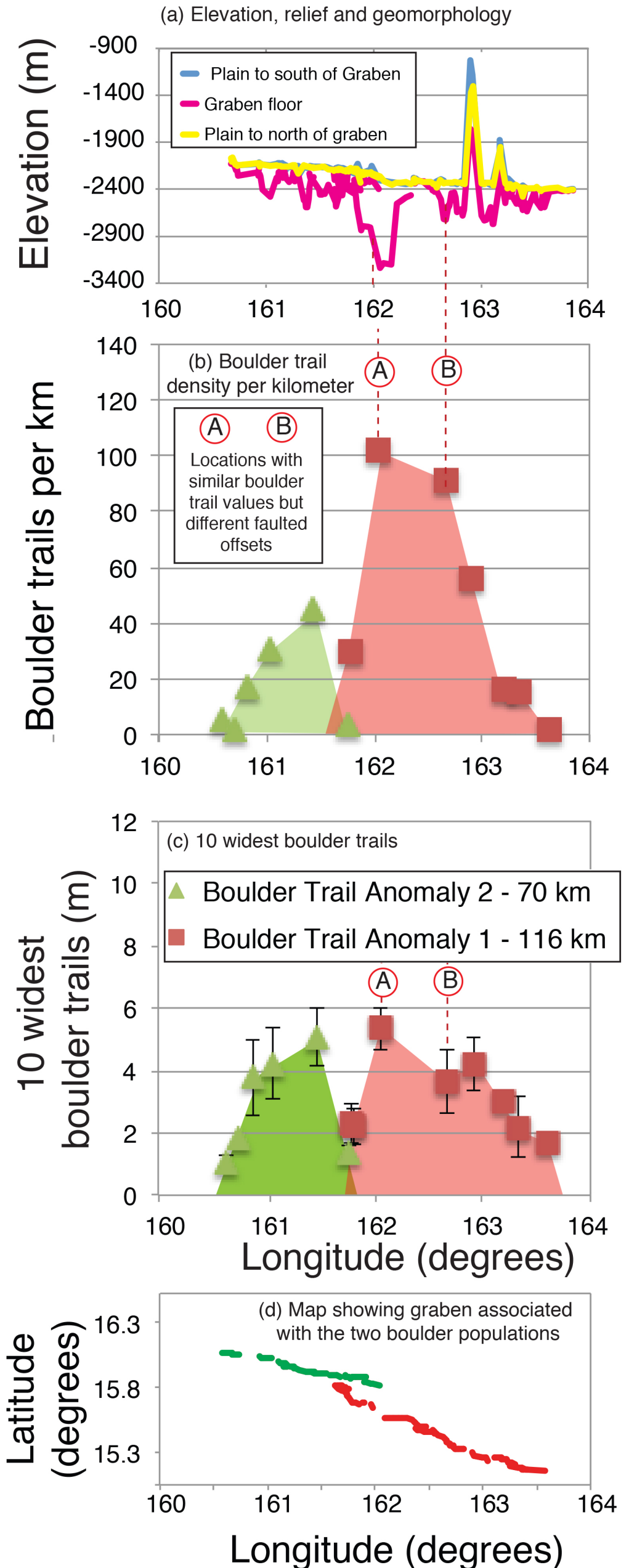
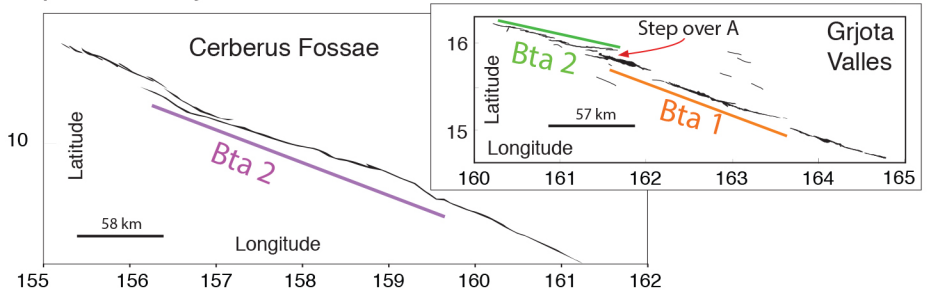


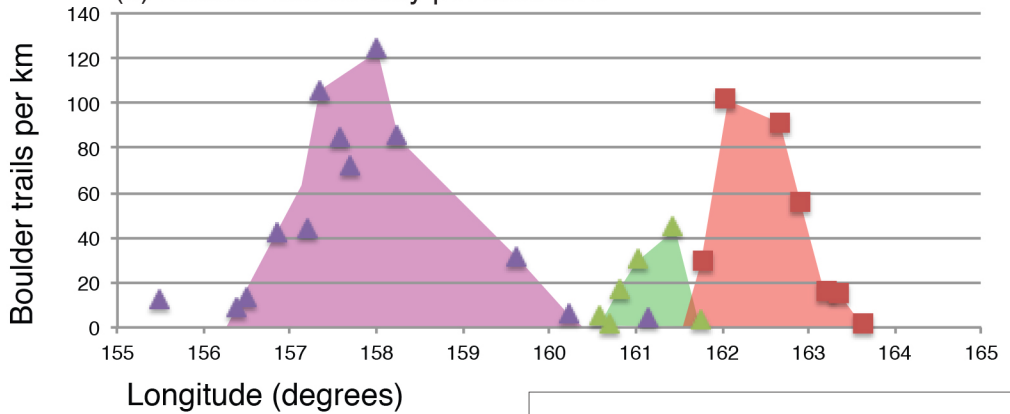


Figure 9

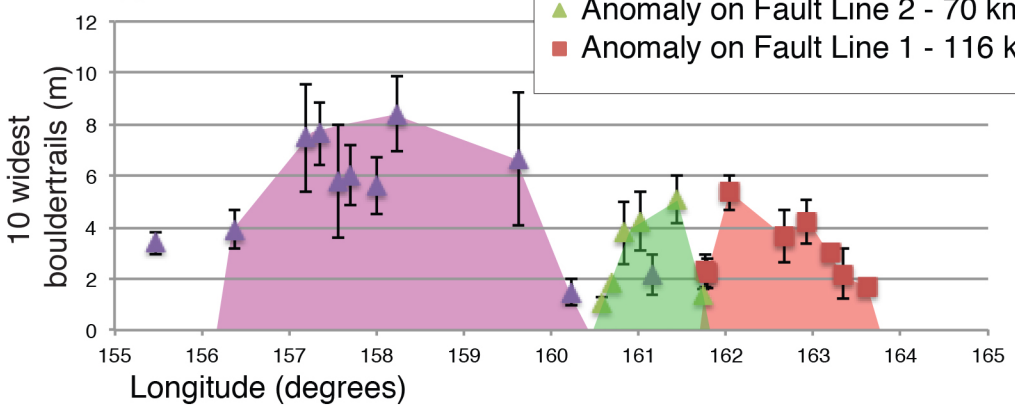
(a) Maps showing the relatively continuous fault length of Cerberus Fossae compared to Grjota Valles and the extent of boulder trail anomalies (Bta).



(b) Boulder trail density per kilometre



(c) 10 widest boulder trails



(d) Speculative inference of marsquake magnitude from rupture length

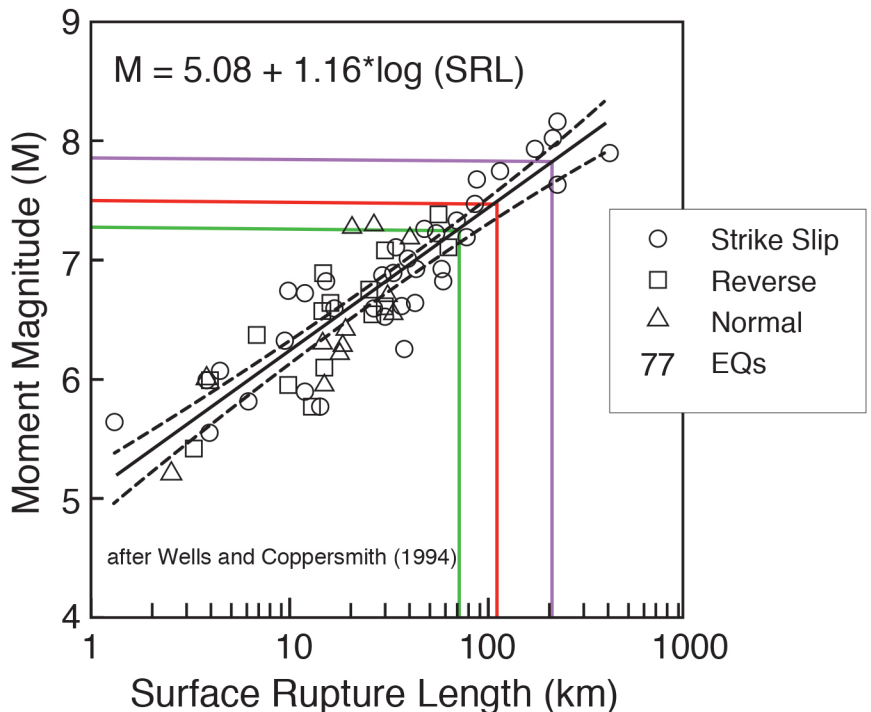
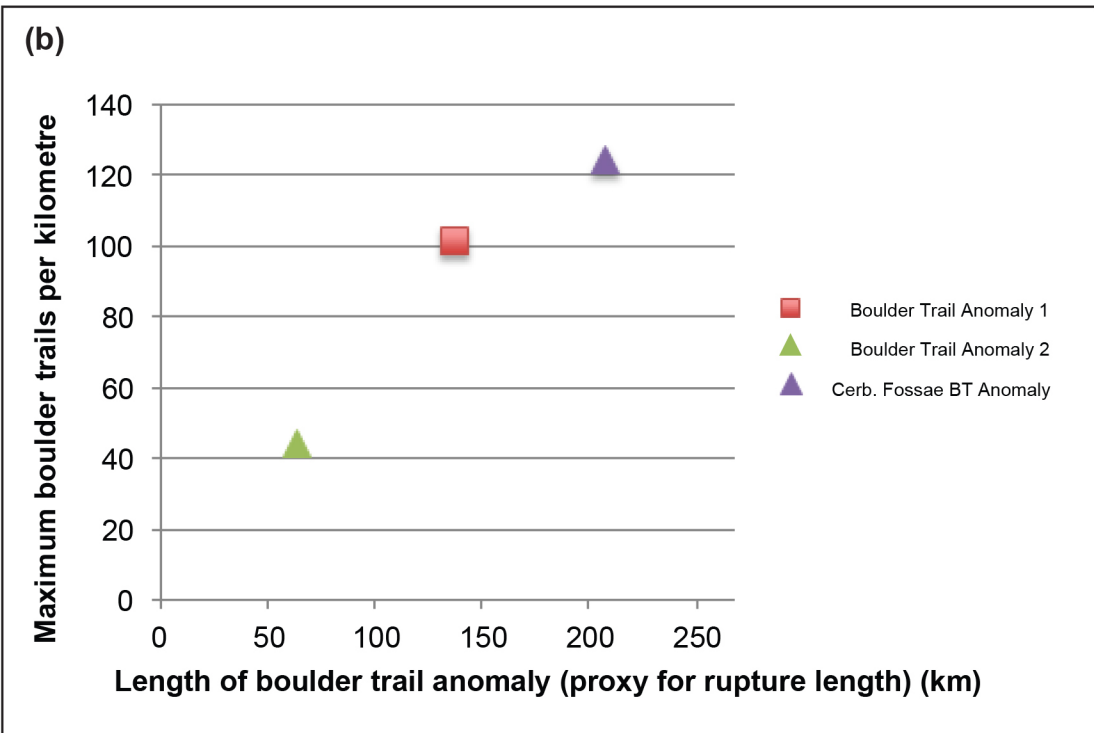
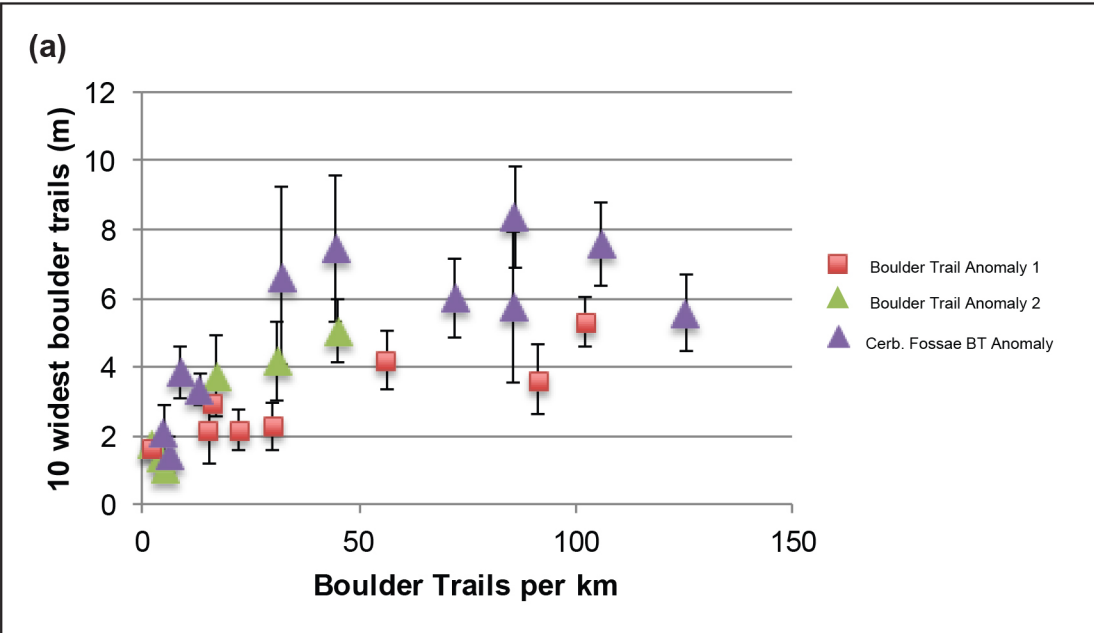
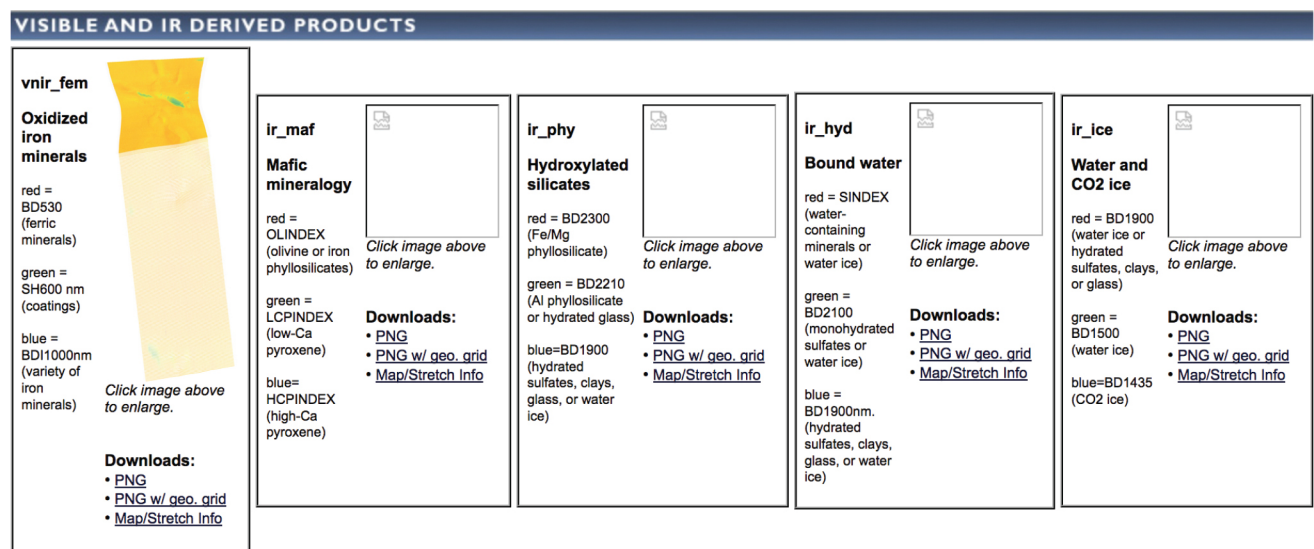
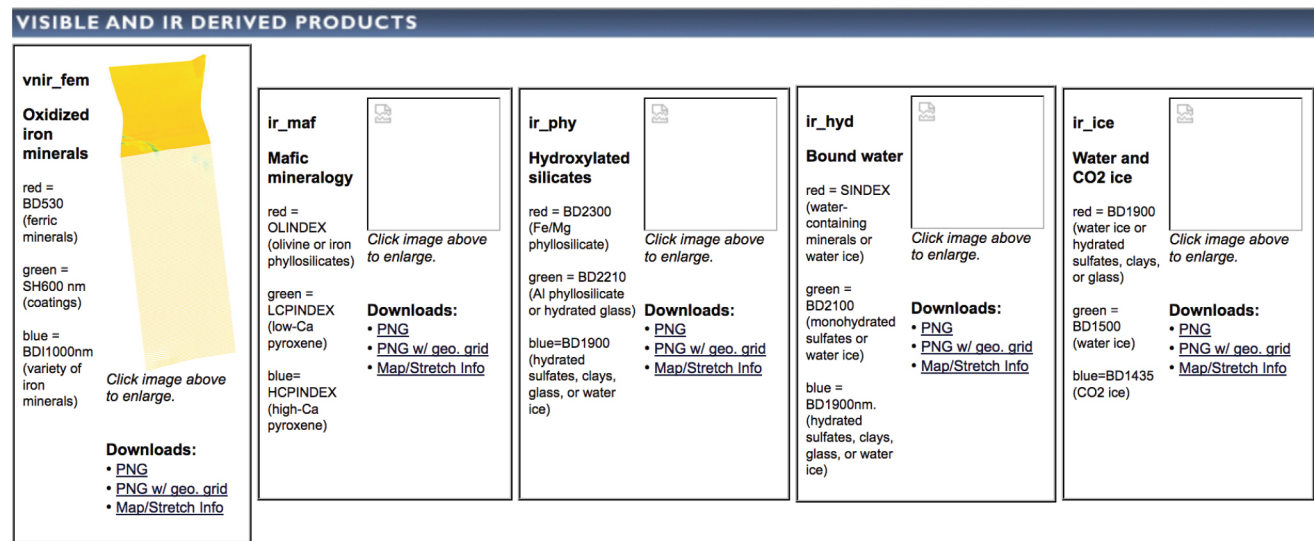
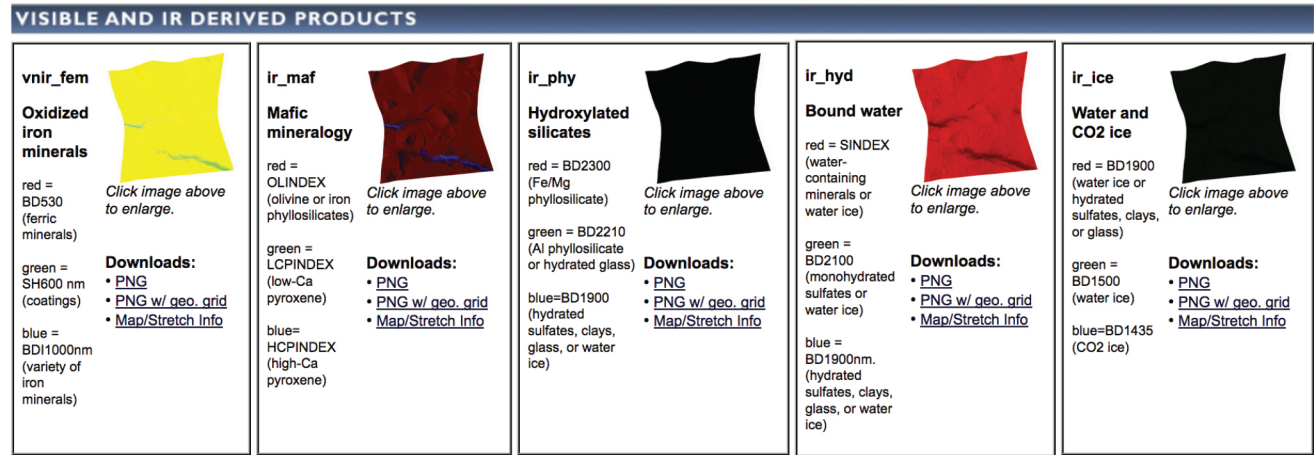


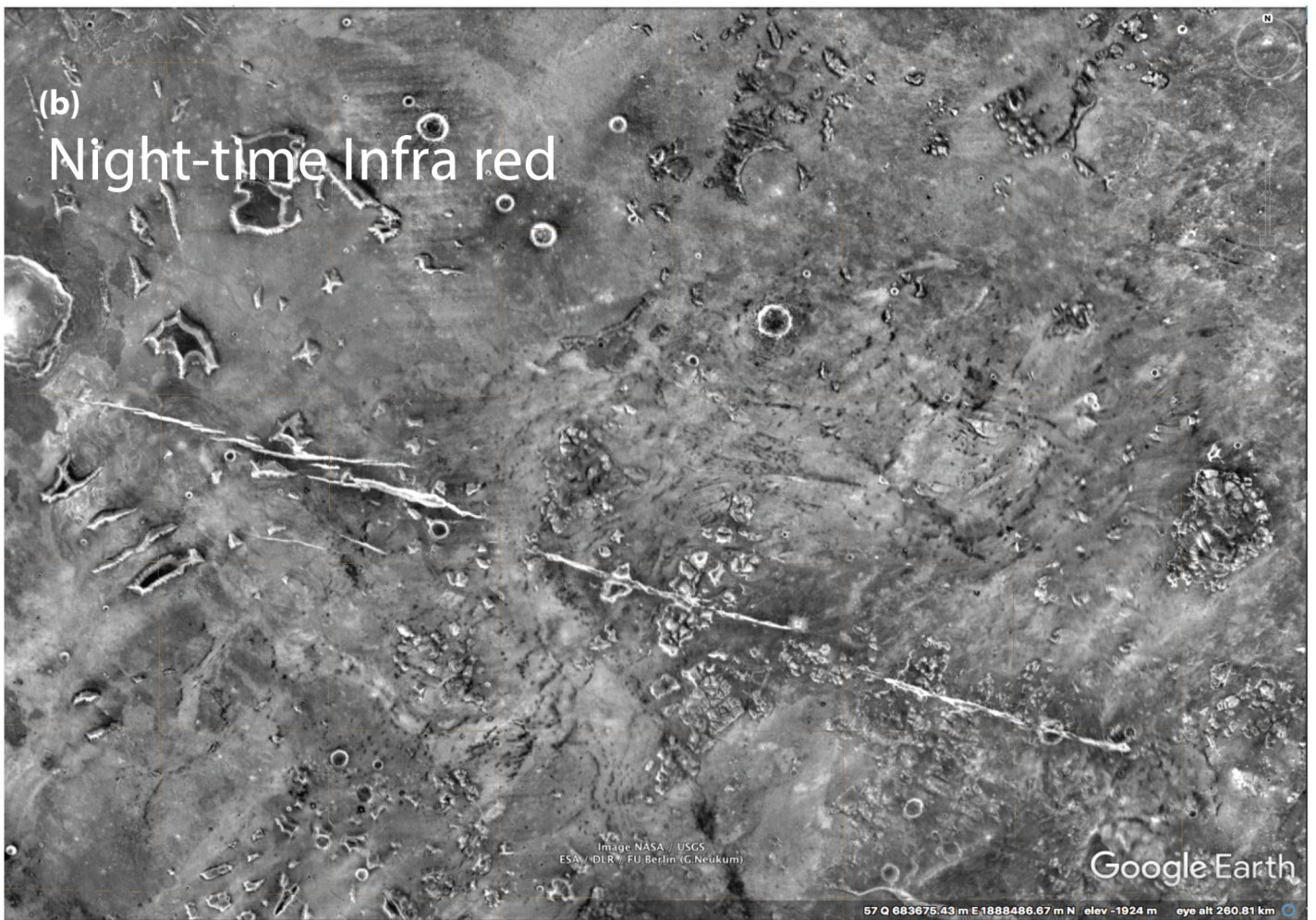
Figure 10





**Supplementary Figure S1:** Relates to the second point for discussion in the Discussion section of our paper, 2) *The effect of local differences lithology and hence weathering/erosion.* The idea that particular lithologies are prone to more or less erosion and as such may control the number and sizes of boulders released from slopes along the graben. S1 is an image from CRISM (Compact Reconnaissance Imaging Spectrometer for Mars) showing that there was no obvious change in the lithology of rocks forming the graben walls. The missing thumbnails are also missing from the CRISM site.





**Supplementary Figure S2:** Relates to the second point for discussion in the Discussion section of our paper, 2) *The effect of local differences lithology and hence weathering/erosion.* The idea that particular lithologies are prone to more or less erosion and as such may control the number and sizes of boulders released from slopes along the graben. S2 a & b are daytime and night-time images from THEMIS (Thermal Emission Imaging System) and shows that there is no obvious change in the lithology of rocks forming the graben walls, highlighting only that the graben walls appear to be formed of bedrock.



# Night-time infrared close-up



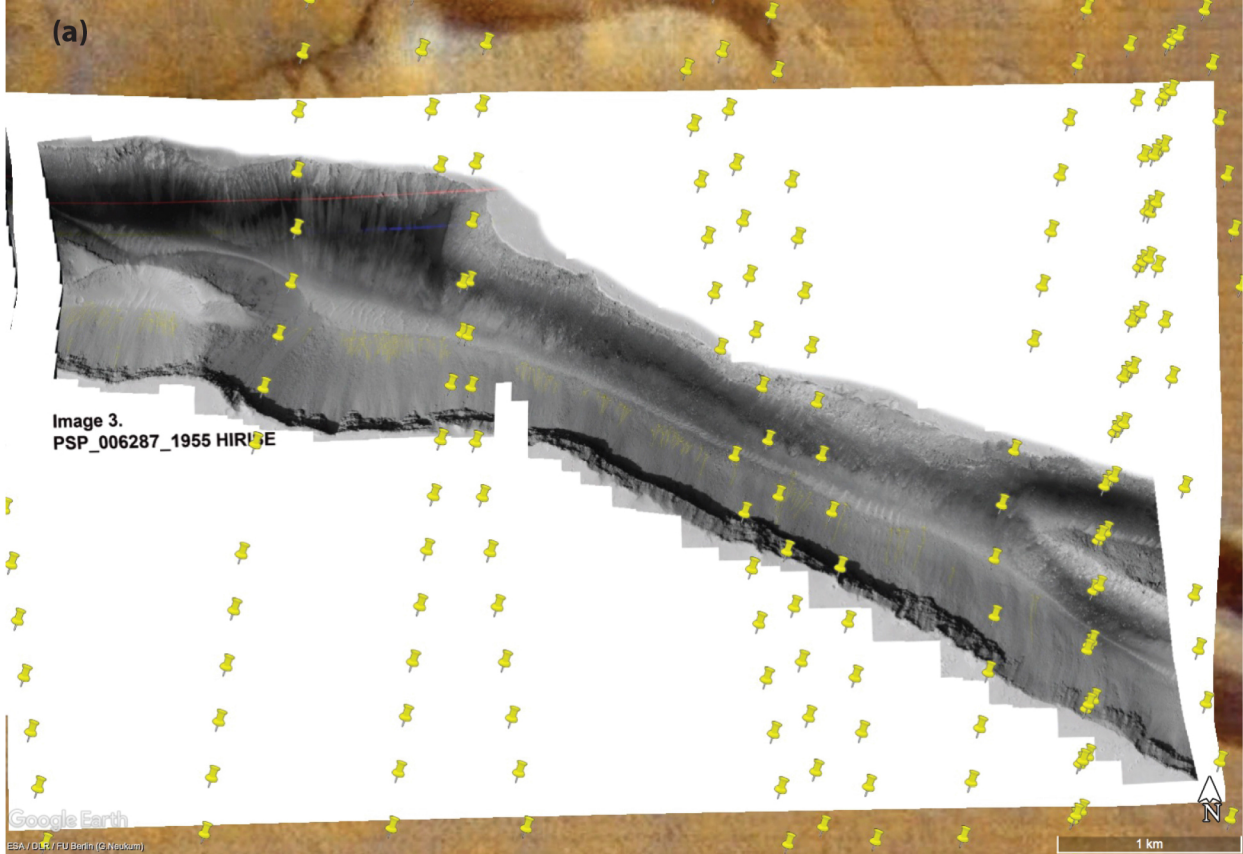
ESA / DLR / FU Berlin (G.Neukum)

Google Earth

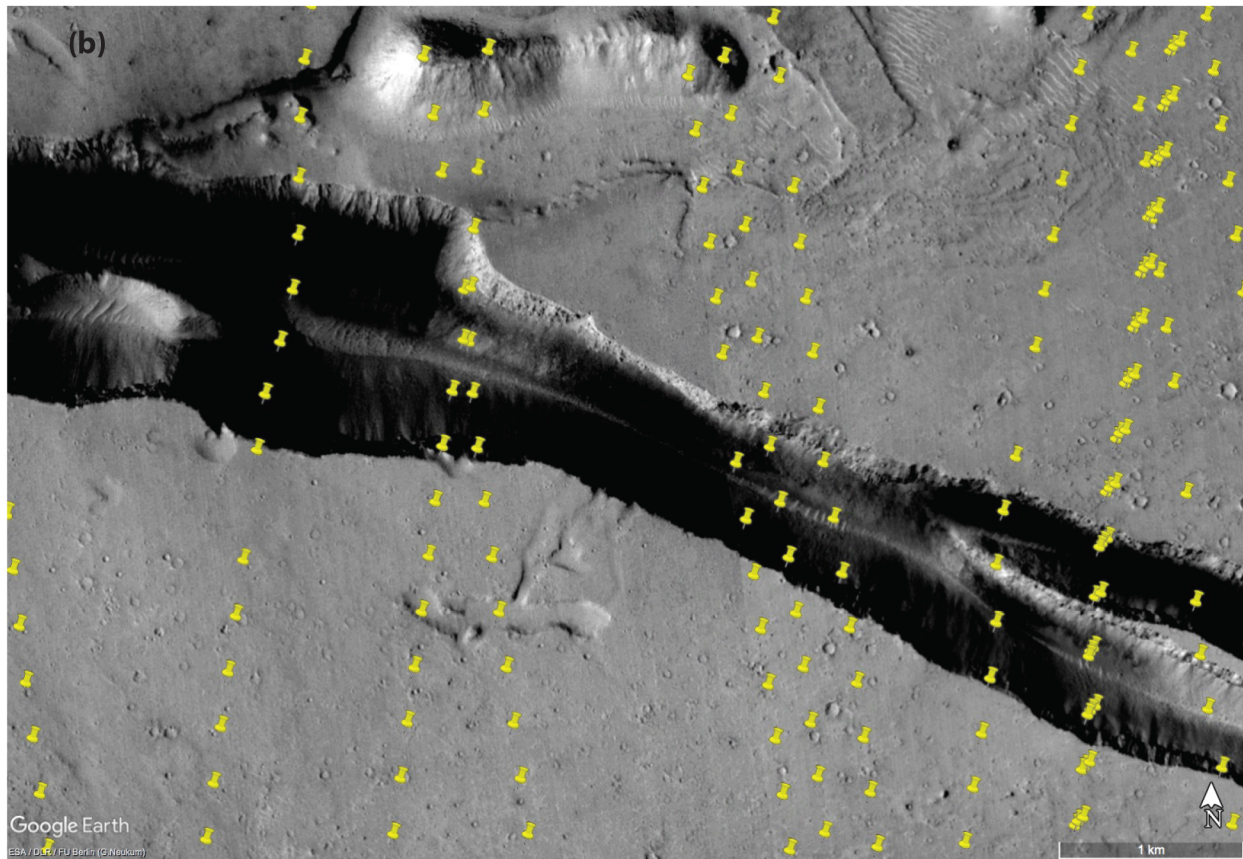
67°Q 747198.41 m E 1799107.27 m N elev -2102 m eye alt 94.14 km

**Supplementary Figure S3:** Relates to the second point for discussion in the Discussion section of our paper, 2) *The effect of local differences lithology and hence weathering/erosion.* The idea that particular lithologies are prone to more or less erosion and as such may control the number and sizes of boulders released from slopes along the graben. S3 a is a close-up night-time infra-red image from THEMIS (Thermal Emission Imaging System) and shows that there is no obvious change in the lithology of rocks forming the graben walls, highlighting only that the graben walls appear to be formed of bedrock.



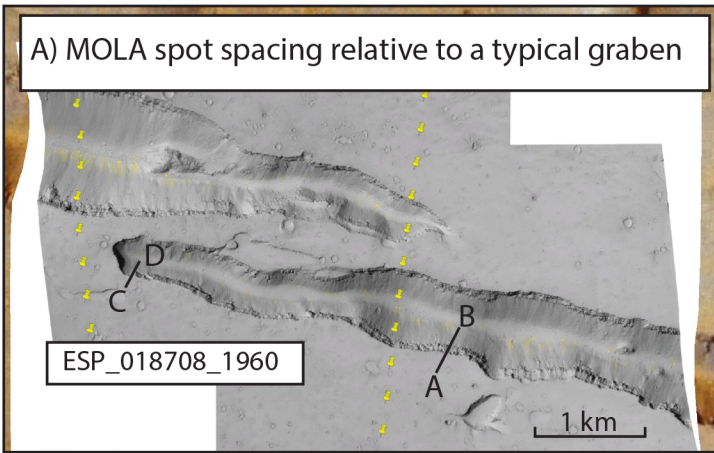


(a) MOLA spacing on HiRISE image



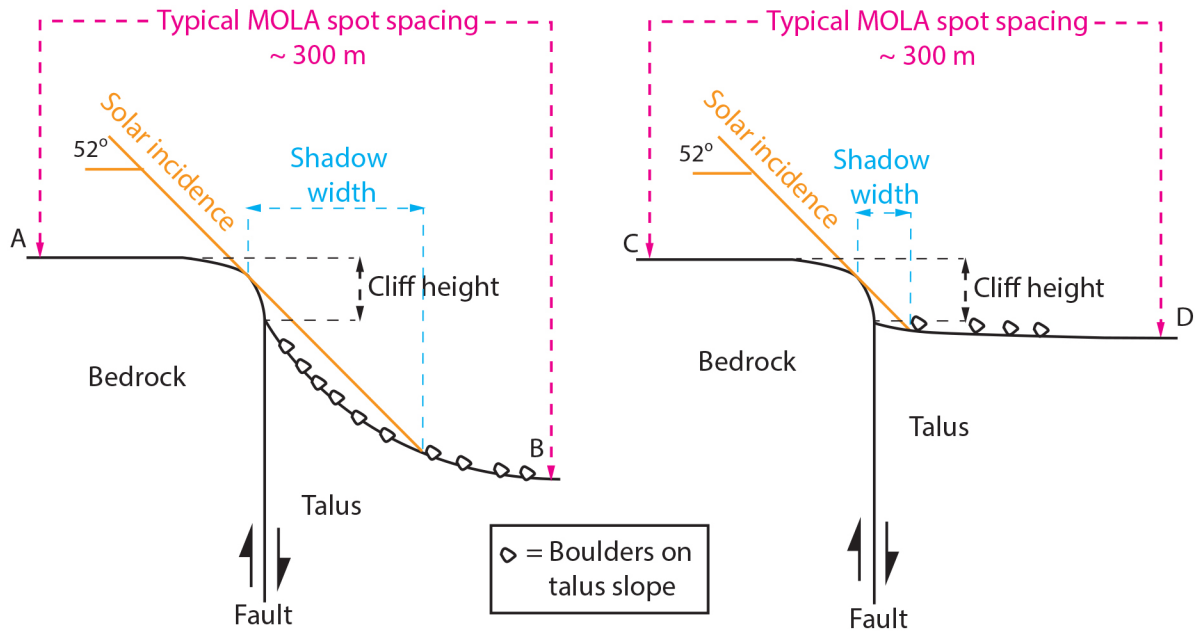
(b) MOLA spacing on CTX image

**Supplementary Figure S4:** Relates to the third point for discussion in the Discussion section of our paper, 3) *Higher cliffs could supply more boulders.* Given that MOLA spot spacing is too coarse ( $\sim 300$  m), measuring the heights and slopes of individual cliffs or talus cones is not possible. S4 (a) (top) shows MOLA spacing on HiRISE image. S4 (b) (bottom) shows MOLA spacing on CTX image.



b) Example with a wide talus slope

c) Example with a narrow talus slope



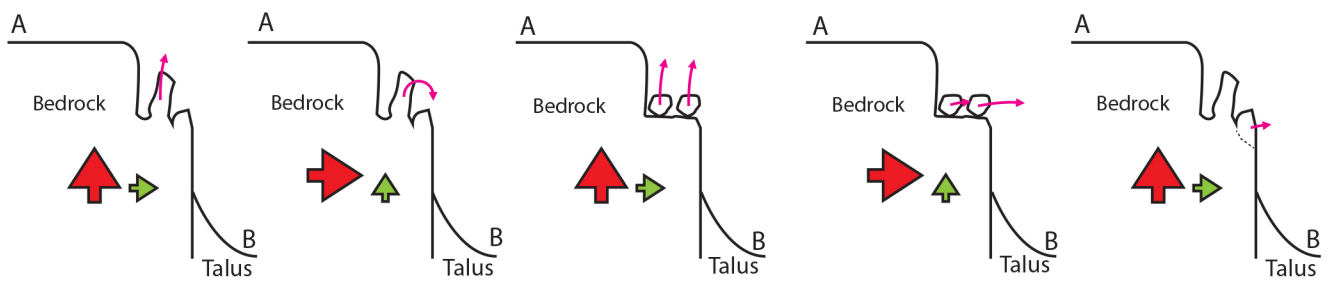
d) Rock pinnacles attached

e) Rock pinnacles toppling

f) Perched Boulders thrown upwards

g) Perched boulders rolling and interacting

h) Boulders detach from rock-mass

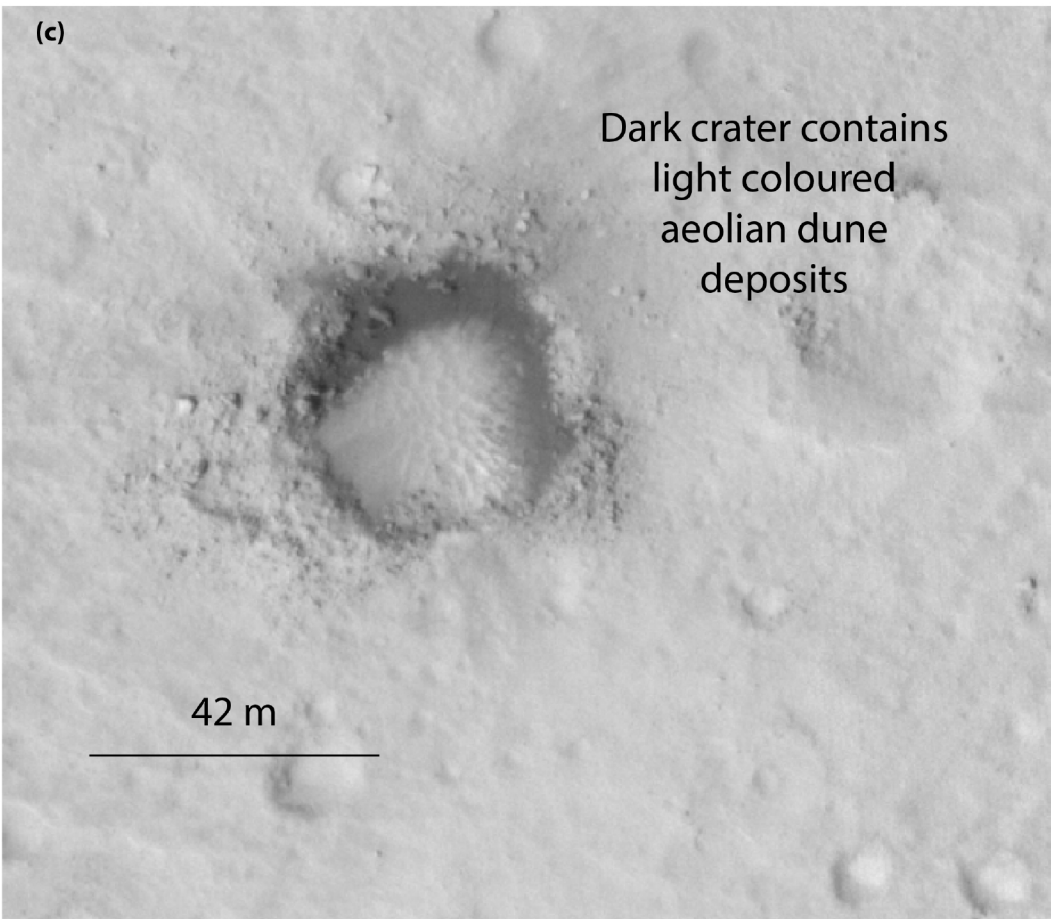
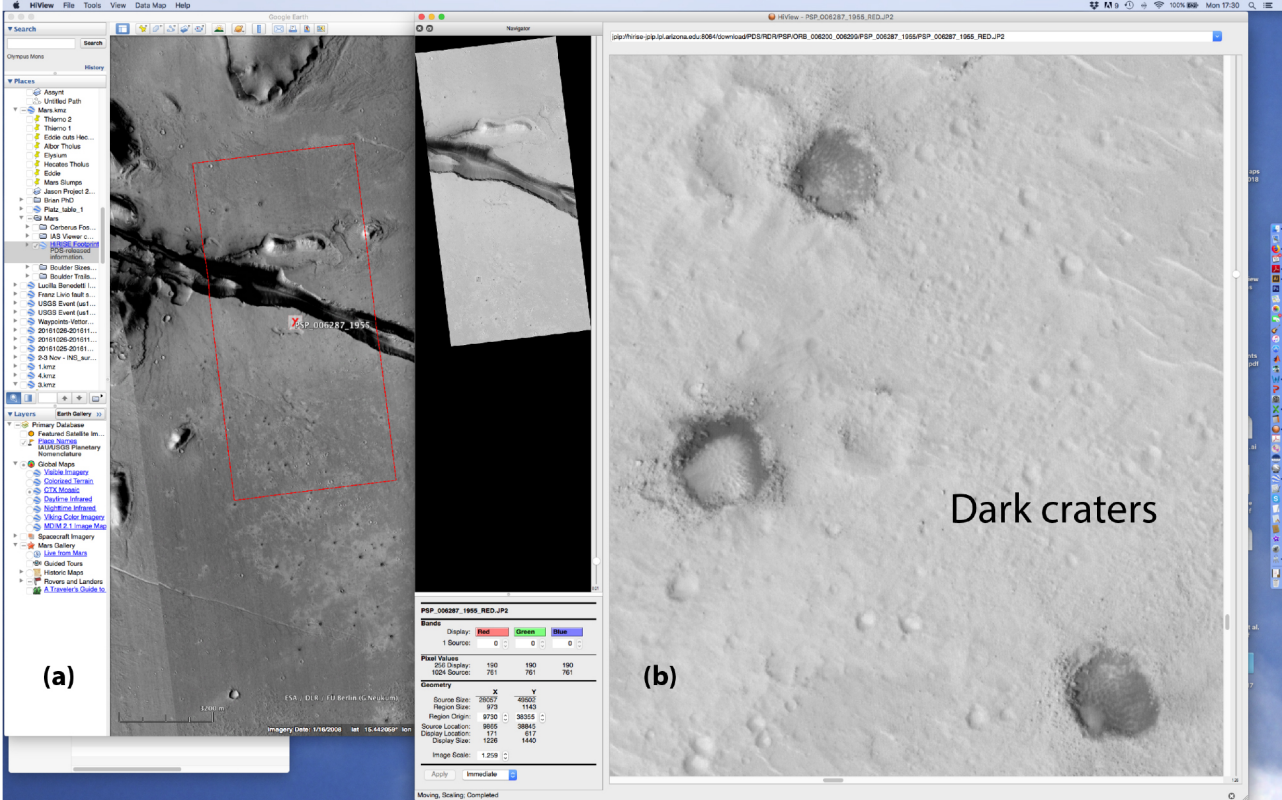


= Vertical acceleration > horizontal acceleration  
 = Horizontal acceleration > vertical acceleration

A — B locates schematic cross-sections

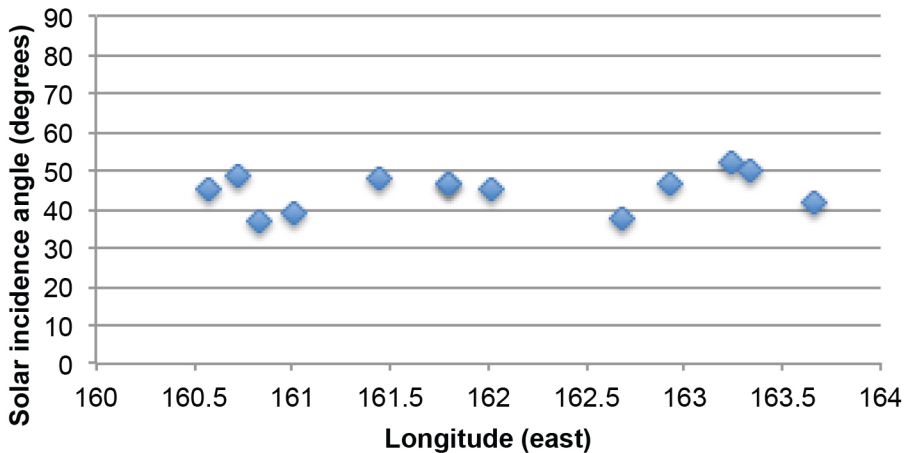
**Supplementary Figure S5:** Relates to the third point for discussion in the Discussion section of our paper, 3) Higher cliffs could supply more boulders and part of the conclusion to our Discussion section related to horizontal or vertical acceleration mobilizing boulders. S5 b and c are diagrams used to illustrate how shadow width and solar incidence angle cannot be used to define vertical height differences via trigonometry, because the horizontal extents of talus slopes vary between different examples. S5 d through h diagrams are to show how weak gravity on Mars may mean that less force is need to mobilize boulders, but it is hard to be precise as this depends on how each boulder was attached and detached, and whether each boulder was mobilized by vertical or horizontal accelerations.





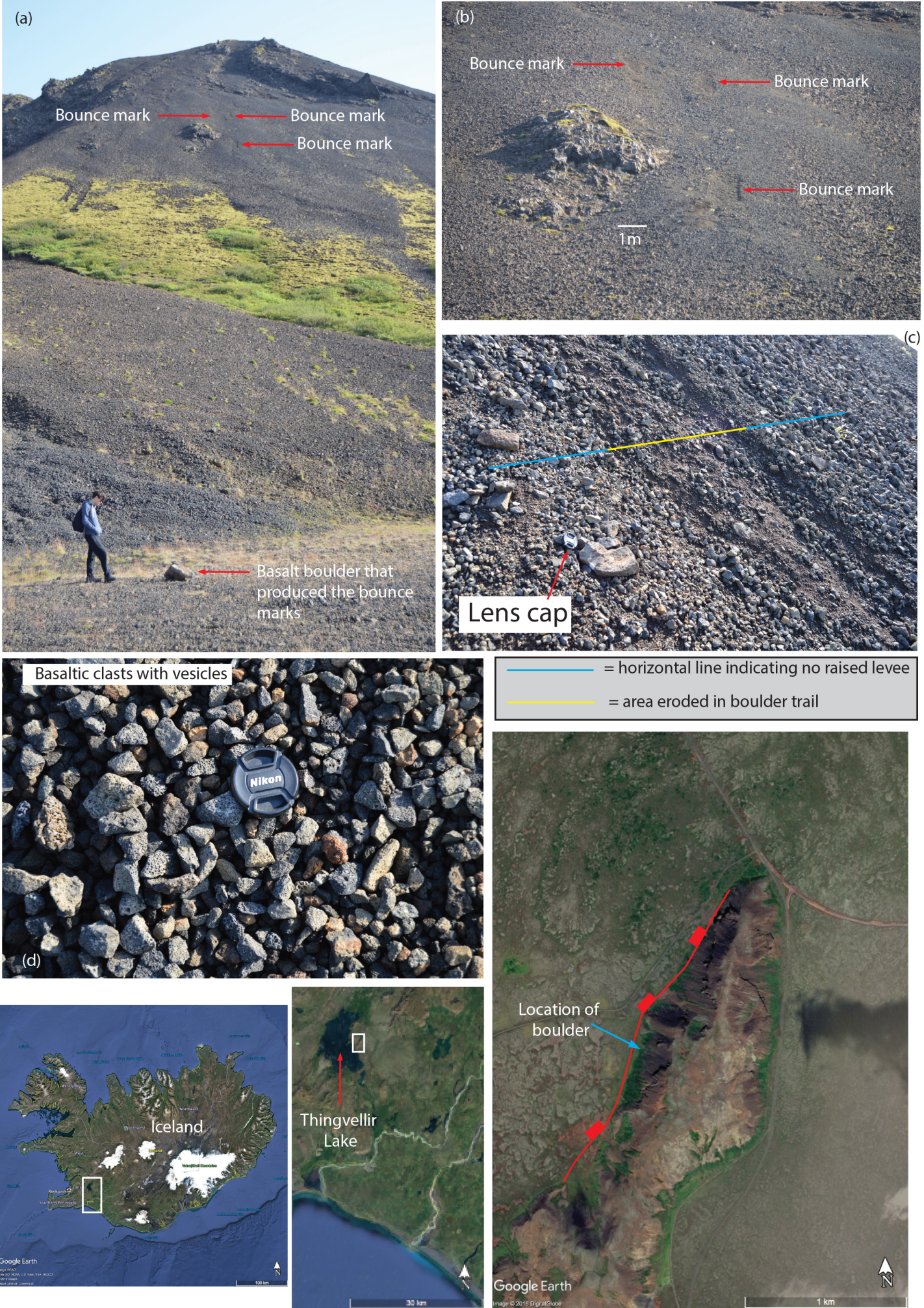
**Supplementary Figure S6:** Relates to the fourth point for discussion in the Discussion section of our paper, *4) Boulder mobilization caused by nearby impacts*. Although some craters near the anomalies appear dark (S6 a & b), and hence perhaps young, when viewed close up (S6 c) they contain dunes indicating that significant aeolian sedimentation has occurred after their formation, indicating they are probably older than the boulder trails which have not been obscured by aeolian processes. S6 a shows the location of the crater in S6 b and c.

## Solar Incidence angle for HiRISE images



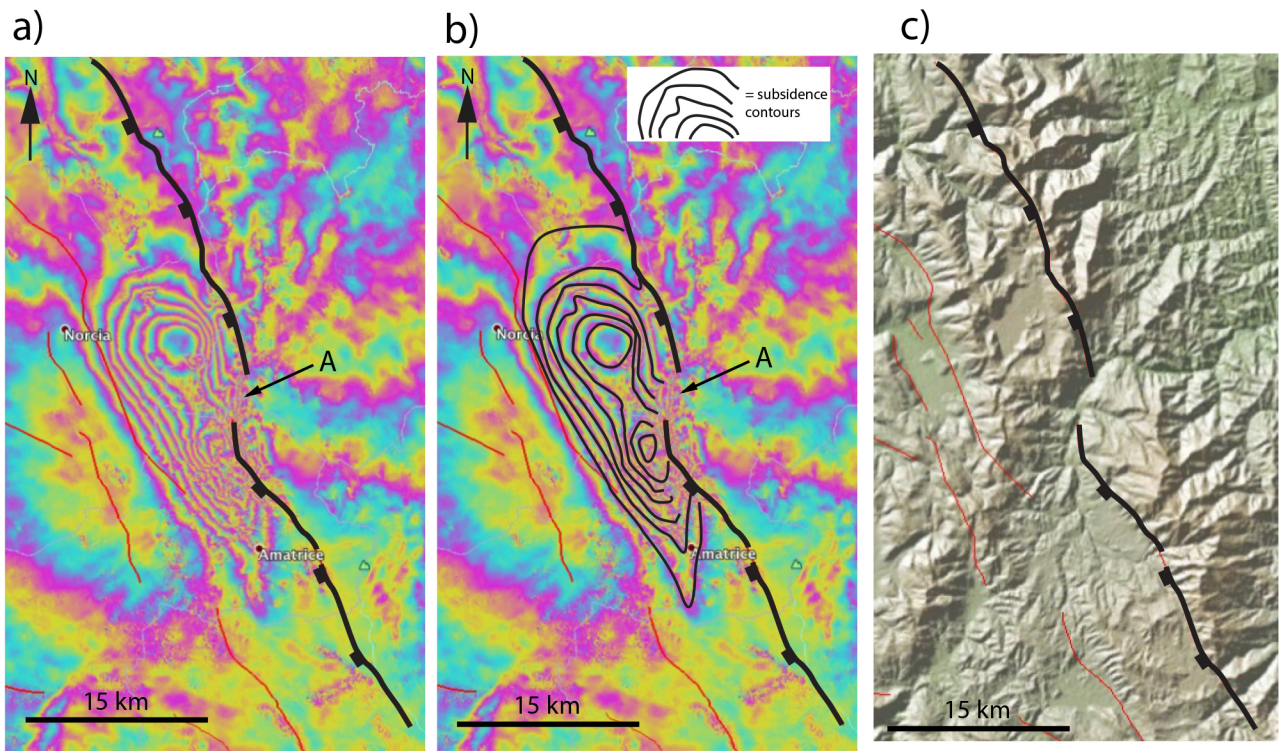
**Supplementary Figure S7:** Relates to the sixth point for discussion in the Discussion section of our paper, 6) Variation in incidence angle of the images makes trails difficult to see. The solar incidence angles for images studied in our paper are similar, as the graph in S7 shows.



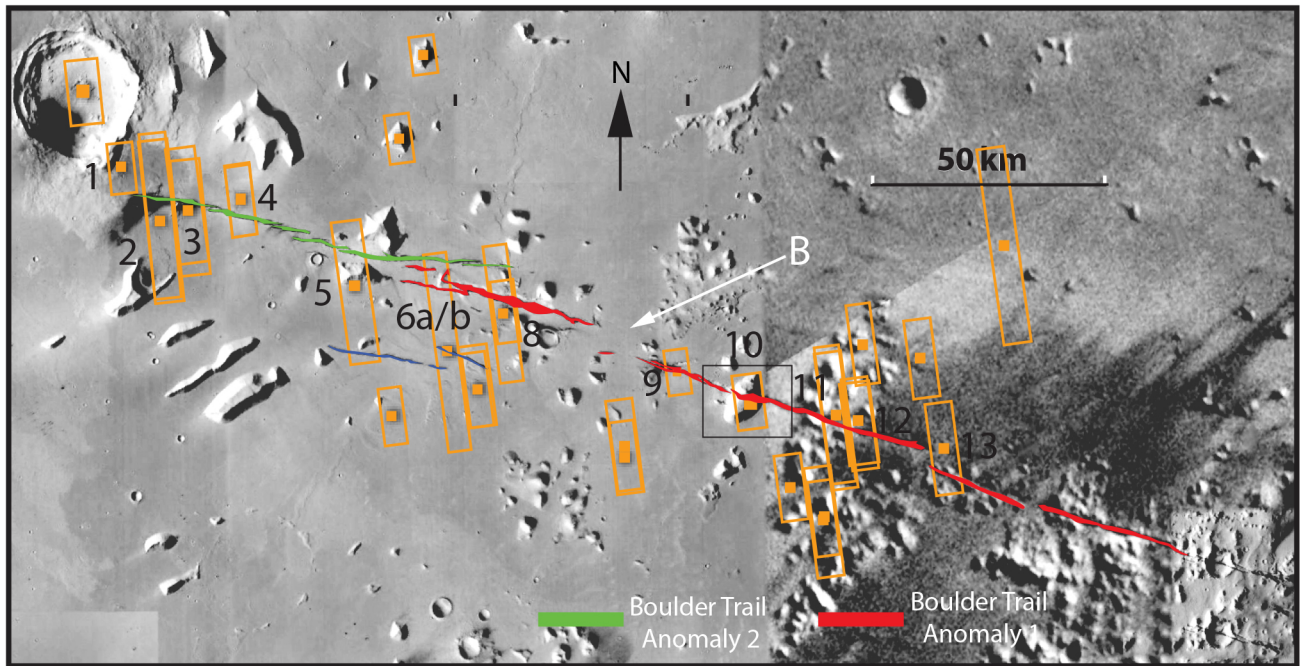


**Supplementary Figure S8:** Relates to the seventh point for discussion in our Discussion section, 7) *The accumulation of boulder trail populations may have developed from multiple single rock falls through time.* Boulder trail examples in Iceland lack raised levees, due to the relatively coarse grain-size. As such, we interpret the grainsize for the examples from Mars as dust to coarse sand. S8 (a), (b), (c) and (d) show boulder trail, bounce marks and boulder. Figures S 8 (e), (f) and (g) are location maps of the boulder trail in S8 (a), (b) and (c).





d)



**Supplementary Figure S9.** (a) and (b) are InSAR data showing the 24th August Mw 6.2 earthquake in central Italy jumping across an area where no surface faulting was reported in the earthquake or on geological maps recording longer term deformation (A), with (c) showing the landscape using an SRTM DEM. This is analogous to the proposed scenario from the fault system in Grjota Valles, (d) where no surface faulting exists on a flat plain (B). InSAR data from <http://comet.nerc.ac.uk/latest-earthquakes-and-eruptions/apennines-earthquakes-aftershocks-italy/> distributed as a kmz file, with one fringe equal to 4.8 cm change in line of sight.